Design and Catalysis of the Attached Nb dimer Catalysts

固定化 Nb ダイマー触媒の設計と触媒作用に関する研究

Nobuyuki ICHIKUNI

一國伸之

Design and Catalysis of the Attached Nb dimer Catalysts

(固定化 Nb ダイマー触媒の設計と
触媒作用に関する研究)

by
Nobuyuki ICHIKUNI

一國　伸之

A Thesis Submitted to The University of Tokyo
for
The Degree of Doctor of Science.

December 1993.

Acknowledgements

First of all, I address my greatest acknowledgement to Prof. Yasuhiro Iwasawa. He introduced me to catalysis field. I would like to acknowledge the continuing guidance and encouragement of Prof. Yasuhiro Iwasawa.

I am grateful to Dr. Kiyotaka Asakura for his warm encouragement and advice especially for EXAFS measurements and analysis. I also thank Dr. Rika Sekine to teach me how to prepare the attached metal catalysts and how to analyse the DV-Xα method. I would like to acknowledge Dr. Tetsuya Aruga, Dr. Hiroshi Onishi and Dr. Takehiko Sasaki for their helpful advises. I wish to thank Mr. Fukui and other members of Prof Iwasawa's Lab., of course including the members already graduated, for their kind support.

Contents

1. General Introduction

1.1. General Remarks

In 1978 none of the world's twenty-five major catalysts contained niobium, on the other hand, catalysts containing molybdenum and vanadium, neighbors of niobium in the periodic table, realized over 80×10^{6} $ of sales in that same year [1].

While niobium has been considered to be an insufficient element for catalysis, thus the amount of catalysts used in industry is so low, it has been demonstrated to possess photocatalytic activity [2], Brönsted acidity [3-5] and unique chemistry in strong metal support interaction (SMSI) phenomena [6-8]. Recently, many niobium-containing catalysts are prepared and investigated, which have been found active for many catalytic reactions.

Niobium oxide in its hydrated form is highly acidic. When used as support, niobium oxide interacts strongly with metal catalysts and affects both reaction activity and selectivity [9-13]. The deposit of niobium oxide on another oxide to form a dispersed surface phase has also led to materials with unusual structural and acidic characteristics. In fact, the entire class of composite oxides, consisting of niobium oxide as one of the components, shows promise as catalysts or catalytic supports. Photocatalytic activity has been reported for silica-supported niobia and layered niobate catalysts.

In the following part of this chapter, I will mention an outline of the chemical properties and catalysis of bulk niobia (1.2), oxide-supported niobia (1.3), mixed oxides containing niobia (1.4) and niobia as a support for metals (1.5).

1.2. Chemical Properties and Catalysis of Bulk Niobia

There have been numerous studies on the structures of Nb_2O_5, and some of the observed structures are well documented [14,15]. Mauerer and Ko synthesized an aerogel of Nb_2O_5 which, after calcination at 773 K for 2 h, remains X-ray amorphous and has a BET surface area of 190 m^2/g. Along with its high surface area, the amorphous Nb_2O_5 aerogel is more acidic than crystalline Nb_2O_5, as shown by n-butylamine titration and pyridine adsorption. They concluded that the origin of acidity is ascribed to NbO_6 octahedra containing Nb=O bonds stabilized in a porous network, leading to strong Lewis acid sites [16].

Surface acidity and basicity investigations have received considerable attention in recent years because they can provide significant information in determining the behavior of solid surfaces [17-21]. Auroux and Gervasini examined the acidity and basicity of a series of metal oxides by using a microcalorimetric technique [22], concluded that Nb_2O_5 is acidic oxides with population of medium-strength acid sites around 60-80 kJ mol^{-1}.

Hydrated niobium pentoxide ($Nb_2O_5 \cdot nH_2O$), which is usually called niobic acid, exhibits a high acid strength (H_o=-5.6) corresponding to the acid strength of 70 % H_2SO_4 when calcined at relatively low temperatures (373-673 K), though the surface of niobic acid calcined at 773 K is almost neutral [3,23,24]. Since any kinds of acidic metal oxides show acidity on calcination at about 773 K and the acidity is lost or decreased by absorbing water, niobic acid which shows the high acid strength on the surface in spite of its containing water is an unusual solid acid. The unusual solid acid is expected to show a stable catalytic acitivity for acid catalyzed reactions in which water

molecules participate or are liberated [25]. Niobic acid is active for ethene hydration [23] and for the vapor phase esterification of ethyl alcohol [4].

Some applications of niobic acid as acid catalyst to organic synthesis have been studied. Phenyloxirane is a useful intermediate in organic synthesis, and its ring-opening reaction is a key step for the utilization. Some solid acids, zeolites and ion exchange resins, were reported as catalyts for the reactions [26,27], but the catalyst performances were not satisfied for an industrial use. By using niobic acid as catalyst, isomerization and hydrolysis of phenyloxirane occurred under mild condtions in high activities and selectivities [28]. The surface hydrophilicity of niobic acid was much more suitable for hydrolysis than that of other solid acid catalysts such as SiO_2-Al_2O_3, H-ZSM5 and H-silicalite, because of the affinity for both water and organic substrate.

There has been a growing interest in process for the dehydrogenation and oxidative dehydrogenation of saturated hydrocarbons. The highest selectivity reported to date for the oxidative dehydrogenation of propane (60 % at a propane conversion of 15 %) was obtained with the V_2O_5/MgO catalyst system [29-31]. Niobium belongs to the same group of periodic system as does vanadium but it is much more inert in its chemistry. Because niobia is less easily reduced than vanadia, it is expected that niobia has different oxidation properties [32]. The oxidative dehydrogenation of propane over the series of oxides, such as lanthana, magnesia, zirconia and titania, Smits *et al.* found that niobia gave the best performance of the series with a selectivity of 76 % to propene and a conversion of propane of 2 % at a temperature of 859 K [33]. Ross *et al.* has

appeared that niobia and niobia-modified catalysts, when used in high-temperature oxidation processes, can exhibit relatively high selectivities compared with more conventional catalysts [34].

Since the pioneer work by Keller and Bhasin [35], a number of catalysts for oxidative coupling of methane have been reported and reviewd [36]. Although aliphatic hydrocarbons are oxidized to CO or CO_2 over Group 5 metal oxides because of their strong oxidation acitivity, it is thought that these metal oxides can be used as promoters for oxidative coupling of methane by controlling the amount of addition to existing catalysts. Especially the increase in catalytic activity is expected. Yamamura *et al.* found that 5 metal oxides containing alkali metal possesses the good result for oxidative coupling of methane but 5 metal oxides alone give poor results [37].

Niobic acid has Brönsted acid sites giving only propene formation upon propan-2-ol conversion and the acidity remains nearly constant with calcination tmeperature up to 673 K where formation of niobic oxide and thus of Lewis-type acid sites occurs [38].

1.3. Oxide-Supported Niobia

1.3.1. Structural characterization

One-atomic-layer metal oxide deposited on high surface area supports may be one of the most promising catalysts from the viewpoint of effective use of resources and may also be of great interest from the viewpoint of new surface chemistry with unique structures [39-53].

Tanaka *et al.* prepared two series of Nb_2O_5/SiO_2 catalysts by an equilibrium adsorption method and a conventional evaporation

to dryness method [54]. UV/VIS diffuse reflectance spectra of the catalyst samples show that micro particles of Nb_2O_5 are present on the catalysts with high-loading and monomeric or oligomeric niobate species are present on the catalysts with low-loading. By analyzing luminescence spectra of the low-loading samples, they concluded that the catalyst prepared by an equilibrium adsorption method contains monomeric NbO_4 tetrahedra and the catalyst prepared by a conventional method contains oligomeric NbO_4 tetrahedra. XANES analysis of the catalysts prepared by a conventional evaporation-to-dryness method has shown that niobium species in Nb_2O_5/SiO_2 is a mixture of octahedrally and tetrahedrally coordinated species [55]. It is very likely that the local structure in the catalysts is influenced by the structure of niobate ions in the impregnation solution. The structure of niobate ions varies with the pH value of the solutions [56].

Supported niobium oxide catalysts were investigated by in situ Raman spectroscopy as a function of Nb_2O_5 loading and oxide support (MgO, Al_2O_3, TiO_2, ZrO_2 and SiO_2) by use of niobium oxalate/oxalic acid aqueous solutions [57] in order to determine the molecular structures of dehydrated surface niobium oxide species [58,59]. On the SiO_2 support, only one dehydrated surface niobium oxide species corresponding to the highly distorted NbO_6 octahedral structure at around 980 cm^{-1} is present. The highly distorted NbO_6 octahedra responsible for Raman bands at *ca.* 985 and 935 cm^{-1} are also observed on the TiO_2 and ZrO_2 supports at high surface coverages. Below half a monolayer coverage on the Al_2O_3 support, two kinds of dehydrated surface niobium oxide species possessing highly and moderately distorted NbO_6 octahedra are present as shown in Figure 1. Upon

approaching monolayer coverage on the Al_2O_3 suport, the Raman band corresponding to highly and slightly distorted NbO_6 octahedra are present suggesting a layered niobium oxide structure. They concluded that dehydrated surface niobium oxide on oxide support is not in tetrahedral symmetry but in octahedral symmetry. It was found that under ambient conditions hydrated hexaniobate-like surface species are present on the alumina support at low surface coverage, while $Nb_2O_5 \cdot nH_2O$, containing slightly distorted NbO_6 as well as NbO_7 and NbO_8 groups, are present at higher surface coverage [60].

In situ XANES/EXAFS studies on the silica-supported niobium oxide catalysts containing different Nb_2O_5 loadings have been reported by Yoshida *et al.* using $YbNbO_4$ and $KNbO_3$ as the reference compounds [61]. They suggest that the dehydrated surface niobium oxide phase possesses a highly distorted NbO_4 tetrahedron at low Nb_2O_5 loadings (< 1 wt%) and a square pyramidal structure at high Nb_2O_5 loadings (> 7 wt%). The proposed dehydrated surface tetrahedral NbO_4 structure consists of one terminal Nb=O bond, with a bond length of 0.177 nm, and three Nb-O bonds, with a bond length of 0.196 nm, coordinated to the SiO_2 surface. At high Nb_2O_5 loadings (> 7 wt%), the proposed dehydrated surface niobium oxide structure consists of one terminal Nb=O bond (0.179 nm), and four Nb-O bond (0.196 nm) coordinated to the SiO_2 surface. The XANES/EXAFS studies on the $YbNbO_4$ reference compound are in agreement with corresponding Raman studies that $YbNbO_4$ consists of a tetrahedral NbO_4 structure [62].

It has been reported that the deposited monolayer phase is stable at elevated temperature, *i.e.* 873 K [63], while amorphous Nb_2O_5 crystallizes into TT- or T-Nb_2O_5 [64]. The Lewis acid

sites in Nb_2O_5/SiO_2 are also considerably more stable than those found in the bulk phase. The Nb_2O_5/SiO_2 prepared from $NbCl_5/CCl_4$+EtOH solution was characterized with various calcination temperatures from 423 to 1573 K [65]. At high calcination temperatures, as T>1473 K, the specific surface area of Nb_2O_5/SiO_2 was nearly reduced to zero as a consequence of crystallization process. Spectroscopic and X-ray diffraction data showed that Nb_2O_5 and SiO_2 crystallized as separated phases at this temperature.

Asakura and Iwasawa prepared one-atomic-layer niobium oxide catalysts supported on silica by use of hexane solution of $Nb(OC_2H_5)_5$ [51-53]. They characterized their catalysts by EXAFS specrocopy and found that surface niobium oxides two-dimensionally grow to cover the silica surface (up to one monolayer). Their result was based on the dependency of total number of Nb-Si bond on the Nb loading detected by EXAFS and the no peaks in the XRD pattern as in Figure 2. They also propose the local structure around Nb atom as shown in Figure 3. Niobic acid layer on SiO_2 were prepared by using $Nb(OC_2H_5)_5$ and characterized by means of EXAFS [39]. Nb-Si bond was also observed, and applied to the proof of the layered growth. The XRD results revealed that the Nb species in Nb_2O_5/SiO_2, prepared from conventional impregnation method by using methanol solution of $NbCl_5$, were aggregated to form three-dimensional T-Nb_2O_5 particles. However, the XRD results showed no peaks corresponding bulk Nb_2O_5 in niobia acid layer on SiO_2, supporting EXAFS result.

Although interactions between niobium oxide and silica are relatively strong, isolated niobium oxide seemed to be not able to prepare on silica surface. However, Nishimura *et al.* prepared

isolated Nb monomer species on SiO_2, Al_2O_3 and TiO_2 by use of $Nb(\eta^3\text{-}C_3H_5)_4$ and characterized by EXAFS [66-68]. After treatment of O_2 at 673 K, the silica attached Nb monomer catalyst possesses tetrahedral structure with two Nb=O double bonds per Nb atom, and the titania attached Nb monomer catalyst also shows tetrahedral struture with one Nb=O double bond and situated as three-fold on titania surface. Their results suggest that niobium oxide can exist on oxide support surface by use of special preparation method, and the structures of NbO_4 unit on supports not depend to Nb loadings (<2 wt%) but the nature of supports.

1.3.2. Acidic properties

Different groups have examined the acidic properties of niobia deposited as a surface phase of oxide onto silica [69-71], magnesia, alumina, titania and zirconia. The surface acidity of solids is critically dependent on the method of the pretreatment used in a particular method [72,73].

It has been reported that the deposited monolayer phase is stable at elevated temperature, *i.e.* 873 K [63], while amorphous Nb_2O_5 crystallizes into TT- or T-Nb_2O_5 [64]. The Lewis acid sites in Nb_2O_5/SiO_2 are also considerably more stable than those found in the bulk phase. For instance, the Lewis acid sites in Nb_2O_5/SiO_2 are stable in samples heated to 800 K [39], while those of Nb_2O_5 are drastically reduced at temperatures above 573 K [3]. Denofre *et al.* investigated the acidic properties of Nb_2O_5/SiO_2 with a low density niobium oxide loading in the temperature range 423-1573 K [65], and found that the Lewis acid sites are stable in samples precalcined up to 973 K and the Brönsted acid sites could be detected for samples precalcined up to 773 K. Nb_2O_5 is known to be a good ion exchanger but is

thermodynamically metastable and can lose its exchange capacity when stored in air [74], but heating the Nb_2O_5/SiO_2 up to 973 K did not affect its transition-metal exchange capacity.

Shirai *et al.* prepared niobic acid layer supported on SiO_2 and examined the acidity by pyridine adsorption [39]. They found that the acidity of Lewis acid site is unchange up to pre-evacuation temperature of 873 K, on the other hand, Brönsted acidity is gradually reduced from pre-evacuation temperature of 473 K to nearly zero at the 673 K. They concluded that the active phase of this catalyst composed of small two-dimensional islands is dispersed on the SiO_2 surface, resulting in the formation of many periphery sites of the niobic acid islands, which also makes the coordinatively unsaturated Nb^{5+} ions with a Lewis acid character.

Burke and Ko have established the acidity-structure relationship of a series of composite containing niobia. Niobia as a tetrahedral species with a Nb=O bond, stabilized by its interaction with silica, shows strong Lewis acidity [69]. This species also has strong Brönsted acidity if it contains terminal hydroxyl groups, as in the case of silica-supported niobia. Octahedral niobia becomes deminant with increasing niobia concentration and/or heat treatment temperature. The highly distorted octahedral species, also with a Nb=O gond, gives moderately strong Lewis acidity whereas the slightly distorted octahderal species gives weak Brönsted acidity. Niobia-silica interactions, which are believed to stabilize the tetrahedral and highly distorted octahedral species, thus lead to enhanced acidity in the composite oxides over the pure oxides. When niobia is the major component, however, the addition of silica does not change the acidic properties significantly because very

little perturvations are introduced into the host matrix.

Datka *et al.* studied the acidic properties of niobium pentoxide supported on silica, magnesia, alumina, titania and zirconia [71]. The infrared spectra of adsorbed pyridine were used to evaluate the concentration and the relative strength of Brönsted and Lewis acid sites. Lewis acidity was found in all the supported niobium oxide systems, while Brönsted acid sites were only detected for niobia supported on the alumina and silica supports. The present of Lewis acid sites can be explained in terms of local coordinative unsaturation of the dopant Nb cations due to specific interactions between the cations and the support. The general predictions from the models that apply Pauling's electrostatic bonding rules [75,76] have been experimentally confirmed, but no theoretical explanation for the surface converage dependence of the Lewis acidity found for the supported niobium oxide catalysts currently exists. However, they found that the acidic characteristics of the Lewis acid site of Nb_2O_5/SiO_2 at the monolayer coverage approach the acidic properties of the Lewis acid sites of bulk Nb_2O_5.

The infrared spectra of the hydroxyl region and that of surface chemisorbed CO_2 apecies for Re_2O_7/Al_2O_3, CrO_3/Al_2O_3, MoO_3/Al_2O_3, V_2O_5/Al_2O_3, TiO_2/Al_2O_3 and Nb_2O_5/Al_2O_3 catalysts have been investigated [77]. Nb_2O_5/Al_2O_3 of lower loadings (3 wt%) possesses no Brönsted acid sites but the largest amount of Lewis acid sites among these catalysts. The case of higher loadings (19 wt%), the number of Brönsted acid sites increases and the Lewis acid sites decreases.

1.3.3. Catalytic properties

The catalysis of supported niobium oxide mainly depends on

its acidity. Various structures were prepared and proposed with different ratio of Lewis acid site and Brönsted acid sites. Thus the catalytic activities dominantly reflect their acidic properties.

The reactivity of the alumina supported niobium oxide catalysts was probed by the methanol oxidation reaction by Jehng and Wachs [78]. The methanol oxidation reaction is very sensitive to the nature of surface sites present in oxide catalysts. Surface redox sites (sites that are capable of being reduced and oxidized) form primarily formaldehyde as well as methyl formate and dimethoxy methane as the reaction products. Surface acid sites, Lewis as well as Brönsted, result in the formation of dimethyl ether. Surface basic sites yield CO/CO_2 as the reaction products. The oxidation of methanol on over the Nb_2O_5/Al_2O_3 yielded dimethyl ether exclusively as the reaction product. Without Nb_2O_5, Al_2O_3 also yielded dimethyl ether, but at a much lower rate. The reactivity of surface niobium oxide species has a slight dependence on surface coverage.

Asakura and Iwasawa examined the catalytic activity for ethanol dehydration and dehydrogenation over the one-atomic-layer niobium oxide supported on silica catalyst, conventional impregnation Nb catalyst and Nb_2O_5 bulk [51-53]. Nb_2O_5 bulk was almost inactive at the temperatures 373-473 K and gave three kinds of products (ethene, diethyl ether and acetaldehyde) unselectively, showing heterogeneous properties of surface. On the other hand, the one-atomic-layer niboium oxide catalyst produced selectively ethene from ethanol over a wide temperature range with activation energy of 16 kJ mol^{-1}. The conventional impregnation Nb oxide catalyst supported on SiO_2 produced dehydration products (ethene and diethyl ether), showing a

similar selectivity to that of Al_2O_3 which is a typical Lewis acid catalyst where at low temperatures diethyl ether is mainly produced and ethene is a main product at higher temperatures.

Monolayer of niobic acid on SiO_2 showed acitivities 20 times as large as that of a niobic acid bulk catalyst for the esterification of acetic acid with ethanol and did not show byproducts such as ethene, diethyl ether and acetaldehyde [39]. The esterification proceeded on the Lewis acid sites which were stable even at 873 K, suggesting the application of this surface layer catalyst in wide reaction conditions.

The low-valent Nb monomer catalysts supported on silica, alumina and titania which were prepared by taking advantage of the reaction between $Nb(\eta^3\text{-}C_3H_5)_4$ and surface OH groups, followed by the treatments with H_2, were found to be active for the hydrogenation of carbon monoxide in which C_2-C_4 hydrocarbons were mainly produced in the temperature range 423-598 K [67]. No formation of CO_2 was observed. In contrast, only the disproportionation reaction of CO to form CO_2 proceeded on conventional impregnation Nb catalysts and bulk Nb_2O_5.

The silica-attached Nb monomer catalyst was found to be the first Nb sample which exhibited a high activity and selectivity for the dehydrogenation of ethanol [68,69]. Although adsorbed ethanol on the catalyst (forming Nb-OH and $Nb\text{-}OC_2H_5$) is too stable to react under vacuum, the catalytic dehydrogenation of ethanol was possible to proceed if in the presence of ambient ethanol showing first sample of self-assisted dehydrogenation mechanism as shown in Figure 4 [69,79]. The results show the switchover of the reaction path from dehydration (γ-hydrogen abstraction) to dehydrogenation (β-hydrogen abstraction) by whether or not ethanol molecules are present in gas phase. The

scission of β-CH bond of a ligand in transition metal complexes has been demonstrated to be accompanied by the presence of d electron and the preferable symmetry of CH antibonding orbital and d occupied orbital [80,81]. The activities of Nb monomers on SiO_2 may be referred to the electron transfer from the surface oxygen 2p level to the Nb 4d level through the Nb-O bonding. The reaction mechanism for the dehydrogenation on the catalyst was entirely different from the dehydrogenation mechanism on the Mo monomer catalyst with a similar structure for the active species; the dehydrogenation of ethanol on Mo sites readily occurred without second ethanol molecules [82].

1.4. Mixed Oxides Containing Niobia

1.4.1. Structural characterization

Niobates have become important ceramic materials owing to their optical and electric properties. For instance, lithium niobate ($LiNbO_3$) has excellent electrooptical, acoustooptical and piezoelectric characteristics [83] and strontium barium niobate ($Sr_xBa_{1-x}Nb_2O_6$) has received great attention as a ferroelectric material [84]. Kominami *et al.* prepared niobium double oxides ($LiNbO_3$, $Zr_6Nb_2O_{17}$, $CaNb_2O_6$, $CrNbO_4$, $FeNbO_4$, $ZnNb_2O_6$ and R_3NbO_7 (R; rare earth)) by use of the glycothermal reaction of niobium alkoxide with suitable alkoxide, acetate or acetylacetone [85]. They characterized the product by use of X-ray diffraction, and estimated the crystallite size from the half-height width of a diffraction peak.

Jehng and Wachs prepared Nb_2O_5/MgO catalysts by use of nonaqueous niobium ethoxide/propanol solutions under a nitrogen environment, and characterized by in situ Raman technique. Their

results showed that the multiple niobium oxide species present are due to the strong acid-base interaction of Nb_2O_5 with the Mg^{2+} and Ca^{2+} contained in MgO cations present on the surface to form $MgNb_2O_6$ and $Ca_2Nb_2O_7$ [58].

$KTiNbO_5$ was prepared by heating an intimate mixture of K_2CO_3, TiO_2 and Nb_2O_5 in the molar ratio of 1:2:1 at 1373 K for 10 h and $HTiNbO_5$ was obtained on HCl treatment of $KTiNbO_5$. Ion-exchange properties of $[TiNbO_5^-]$ layers were reported [86] and aliphatic amine intercalates have been investigated [87]. Tagaya *et al.* examined intercalation of organic compounds into these layered titanoniobate [88]. They measured interlayer spacing by use of latice parameters determined from XRD, and showed how widely changes the interlayer separation by introducing different organic compounds.

1.4.2. Acidic properties

The layered compounds are written by the general formula, $ALaNb_2O_7$, and their catalytic properties have been hardly investigated. The compounds are built up of the layer compound, $LaNb_2O_7$, having double perovskite structure which are interleaved by A atoms. In the case of A=H it is known that the compound has water in the interlayer and exhibits the acidic property [89]. Since the water in the interlayer of montmorilonite dissociates 10^7 higher than liquid water [90], it is also considered that the water in the interlayer will be concerned with the acidic properties of $HLaNb_2O_7$. Acidic properties of $HLaNb_2O_7$ catalyst treated at various temperatures are investigated by Matsuda *et al.* [91]. When the $HLaNb_2O_7$ catalyst was dipped in water, the suspended solution exhibited the acidic pH values by the dissociation of proton in the catalyst. The dissociation may be

due to the action of the water intercalated into the interlayer. With raising the treatment temperature, the pH value turned to the higher values, which would be ascribed to the decrease of the amount of the water in the interlayer.

1.4.3. Catalytic properties

It had been previously shown that the addition of niobium oxide to a mixture of molybdenum and vanadium oxides improves the activity of this system for the oxidative dehydrogenation of ethane [92]. Further investigation on the oxidative dehydrogenation of ethane has been studied using molybdenum-vanadium-niobium oxide catalysts in the temperature range 623-723 K by Desponds *et al.* [93]. Their results suggest that active phase is based on molybdenum and vanadium, and the introduction of niobium enhances the intrinsic activity of the molybdenum-vanadium combination and improves the selectivity by inhibiting the total oxidation of ethane to carbon dioxide. The best results have been obtained using a mixture having a Mo:V:Nb ratio of 19:5:1.

Smits *et al.* investigated systematically on the performance of oxidation of propane over vanadium-niobium-oxide catalysts [94]. They assumed that the active site is a vanadium ion at the surface, and that the activity and selectivity of this active site depends on the number of neighbouring vanadium and niobium ions. Neighbouring vanadium ions provide additional activity, while neighbouring niobium ions improve the selectivity. The optimal activity and selectivity are given by a site having both vanadium and niobium as neighbours (V-O-V*-O-Nb).

On the basis of the results of the intercalation of water, dehydration of 1-butanol on the $HLaNb_2O_7$ catalyst was attempted

[91], because the reaction would proceed on the acidic sites [95]. The results of the reaction of 1-butanol at the temperature range between 473 and 623 K are summarized as follows: The formation of 1-butene was predominant at 473 K, although the equilibrium composition of dehydration products of 1-butanol was calculated as 1-butene : trans-2-butene : cis-2-butene = 26.4 : 53.1 : 20.5, respectively. Though the selectivity to butenes increased with raising the reaction temperature, the experimental results were entirely contrary to the calculation. By the heat treatment of the catalyst at 673-773 K, the activity for the reaction at 473 K remarkably decreased, but the selectivity to n-butylaldehyde was attained to *ca.* 100 %. This result suggests that the formation of n-butylaldehyde is not concerned with the acidic property of the catalyst.

Bi-Mo-based composite oxides are well known as the catalysts for the partial oxidation and ammoxidation of lower olefins. Particularly, they are industrially important for the synthesis of acrolein by oxidation of propylene and of acrylonitrile by ammoxidation of propylene. Recently, many patents on the synthesis of acrylonitrile by the ammoxidation of propane instead of propylene and the catalysts for their sysnthesis have been claimed. Kim *et al.* proposed that Scheelite-type Bi-Mo-based oxides containing Nb, Ta or V ions are highly active catalysts for synthesizing acrylonitrile by the ammoxidation of propane [96]. Matsuura *et al.* found that the mixed catalyst composed of Bi-Mo-based composite oxides and amorphous Nb_2O_5 and that supported by γ-Al_2O_3 and SiO_2 which have strong acid properties were improved in their catalytic activities with keeping of their selectivity for ammoxidation of isobutane to methacrylonitrile

and presented the reaction scheme as Figure 5 [97].

1.5. Niobia as a Support for Metals

Supported metals are used extensively as heterogeneous catalysts, the traditional role of the support being to disperse and stabilize the small metal particles. Strong metal support interactions (SMSI) have been found for many metals supported on reducible transition metal oxides after reduction at moderately high temperatures [98,99]. The work of Tauster *et al.* showed that hydrogen chemisorption is suppressed on group 8-10 metals supported on a series of oxides after these samples have been reduced at high temperatures by hydrogen [6,7]. The term SMSI was introduced to describe this behavior.

Metals supported on TiO_2 have a greatly reduced capacity to adsorb H_2 or CO after reduction at temperatures above *ca.* 750 K, these phenomena was also observed in metals supported on Nb_2O_5 [8-13,100]. The hydrogen adsorption is suppressed after reduction at high temperatures, there being a large decrease for 10 wt% Ni/Nb_2O_5 as the ratio of the number of H atom to surface nickel atom is 0.16 and 0.02 for reduced at 573 K and 773 K, respectively [101]. These results compared with similar data previously obtained for TiO_2 supported nickel catalysts [102] showed that Nb_2O_5 was more interacting support than TiO_2 for nickel, when parameters such as average crystallite size and reduction treatment were comparable [101]. Kunimori *et al.* have compared the SMSI behavior of Rh/Nb_2O_5 and Rh/TiO_2 for both CO hydrogenation [103] and ethane hydrogenolysis [104] and have noted differences in the nature of SMSI. Particularly noteworthy is the suppression in the CO hydrogenation activity on Rh/Nb_2O_5

after HTR. Kunimori *et al.* reported that the Rh-Nb_2O_5 interaction increases with the temperature of calcination as evidenced by the formation of $RhNbO_4$ phase, identified by X-ray diffraction, when Nb_2O_5-promoted Rh/SiO_2 catalysts are calcined at 973 K [105]. Subsequent TPR studies indicate that as the Rh-Nb_2O_5 interaction increases, the Rh becomes more difficult to reduce.

In general, the SMSI effect has a great influence on structure-sensitive reactions but only a minor effect on structure-insensitive reactions [99,106]. By use of Nb_2O_5 supported Pd, Pd-Cu catalysts, Pereira *et al.* concluded that 1,3-butadiene hydrogenation is a structure sensitive reaction [107]. Catalytic activities of typical structure sensitive reactions such as hydrogenolysis of C_2H_6 and *cyclo*-C_6H_{12} on Rh/Nb_2O_5 catalyst were suppressed by 5 to 6 orders of magnitude by high-temperature reduction (HTR), whereas a suppression is only by about 1 order of magnitude in a *cyclo*-C_6H_{12} dehydrogenation on Rh/Nb_2O_5 catalyst as a structure insensitive reaction [108].

Aranda *et al.* evaluated the catalytic properties of niobia and alumina-supported platinum and platinum-tin catalysts at the conversion of n-heptane at 773 K, and concluded that the high selectivity for olefin formation is due to the ensemble effect of partially reduced support and to the formation of active sites at metal-support interface and the presence of tin decreased the SMSI state, causing a decrease in the olefin/toluene ratio [109].

References

[1] C.J.Wright and W.A.England, *Niobium, Proc. Int. Symp. 1981*, (1984)561.

[2] Y.Wada and A.Morikawa, *Bull. Chem. Soc. Jpn.*, **60**(1987)3505.

[3] T.Iizuka, K.Ogasawara and K.Tanabe, *Bull. Chem. Soc. Jpn.*, **56**(1983)2927.

[4] Z.Chen, T.Iizuka and K.Tanabe, *Chem. Lett.*, (1984)1085.

[5] T.Iizuka, S.Fujie, T.Ushikubo, Z.Chen and K.Tanabe, *Appl. Catal.*, **28**(1986)1.

[6] S.J.Tauster, S.C.Fung and R.L.Garten, *J. Am. Chem. Soc.*, **100**(1978)170.

[7] S.J.Tauster and S.C.Fung, *J. Catal.*, **55**(1978)29.

[8] E.I.Ko, J.E.Lester and G.Marcelin, *Strong Metal-Support Interactions, ACS Symp. Ser.* No. 298, (1986)123.

[9] E.I.Ko, M.Hupp and N.J.Wagner, *J. Catal.*, **86**(1984)315.

[10] K.Kunimori, Y.Doi, K.Ito and T.Uchijima, *J. Chem. Soc., Chem. Commun.*, (1986)965.

[11] H.Yoshitake, K.Asakura and Y.Iwasawa, *J. Chem. Soc., Faraday Trans. 1*, **84**(1988)4337.

[12] H.Yoshitake, K.Asakura and Y.Iwasawa, *J. Chem. Soc., Faraday Trans. 1*, **85**(1989)2021.

[13] H.Yoshitake and Y.Iwasawa, *J. Catal.*, **125**(1990)227.

[14] H.Schäfer, R.Gruhen and F.Shulte, Ang. Chem., Internat. Ed. Engl., 5(1966)40.

[15] K.Kato and S.Tamura, *Acta. Cryst.*, **B31**(1975)673; K.Kato, *Acta. Cryst.*, **B32**(1976)764.

[16] S.M.Mauerer and E.I.Ko, *J. Catal.*, **135**(1992)125.

[17] J.Kijenski and A.Baiker, *Catal. Today*, **5**(1989)1.

[18] K.Tanaka and A.Ozaki, *J. Catal.*, **8**(1967)1.

[19] V.C.F.Holm, G.C.Bailey and A.Clark, *J. Phys. Chem.*, **63**(1959)129.

[20] K.H.Bourne, F.R.Cannings and R.C.Pitkethly, *J. Phys. Chem.*, **74**(1970)2197.

[21] B.Imerik, C.Naccache, G.Courdurier, Y.Ben Taarit and J.C.Vedrine (eds.), *Catalysis by Acids and Bases, Stud. Surf. Sci. Catal.*, Vol. 20, Elsevier, Amsterdam, 1985.

[22] A.Auroux and A.Gervasini, *J. Phys. Chem.*, **94**(1990)6371; A.Gervasini and A.Auroux, *J. Catal.*, **131**(1991)190.

[23] K.Ogasawara, T.Iizuka and K.Tanabe, *Chem. Lett.*, (1984)645.

[24] K.Tanabe, *Chemtech*, **21**(1991)628.

[25] K.Tanabe, *Catal. Today*, **8**(1990)1.

[26] G.Paparatto and G.Gregorio, *Tetrahedron Lett.*, **12**(1988)1471.

[27] G.A.Olah, A.P.Fung and D.Meider, *Synthesis*, (1981)280.

[28] T.Hanaoka, K.Takeuchi, T.Matsuzaki and Y.Sugi, *Catal. Today*, **8**(1990)123.

[29] M.A.Chaar, D.Patel, M.C.Kung and H.H.Kung, *J. Catal.*, **105**(1987)483.

[30] M.A.Chaar, D.Patel and H.H.Kung, *J. Catal.*, **109**(1988)463.

[31] D.Siew Hew Sam, V.Soenen and J.C.Volta, *J. Catal.*, **123**(1990)417.

[32] R.H.H.Smits, K.Seshan and J.R.H.Ross, *J. Chem. Soc., Chem. Commun.*, (1991)558.

[33] R.H.H.Smits, K.Seshan and J.R.H.Ross, *ACS Petrol. Chem. Div. Prepr.*, **37**(1992)1121.

[34] J.R.H.Ross, R.H.H.Smits and K.Seshan, *Catal. Today*, **16**(1993)503.

[35] G.E.Keller and M.M.Bhasin, *J. Catal.*, **73**(1982)9.

[36] Y.Amenomiya, V.I.Birss, M.Goledzinowski, J.Galuszka and

A.R.Sanger, *Catal. Rev. -Sci. Eng.*, **32**(1990)163.

[37] M.Yamamura, H.Okado and N.Tsuzuki, *Chem. Lett.*, (1992)203.

[38] A.Ouqour, G.Coudurier and J.C.Vedrine, *J. Chem. Soc., Faraday Trans.*, **89**(1993)3151.

[39] M.Shirai, K.Asakura and Y.Iwasawa, *J. Phys. Chem.*, **95**(1991)9999.

[40] A.Vejux and P.Courtine, *J. Solid State Chem.*, **23**(1978)93.

[41] M.Inomata, K.Mori, A.Miyamoto, T.Ui and Y.Murakami, *J. Phys. Chem.*, **87**(1983)754.

[42] M.Niwa, S.Kato, T.Hattori and Y.Murakami, *J. Chem. Soc., Faraday Trans. 1*, **80**(1984)3135.

[43] I.E.Wachs, R.Y.Saleh, S.S.Chan and C.Chersich, *Appl. Catal.*, **15**(1985)339.

[44] I.E.Wachs, R.Y.Saleh, S.S.Chan and C.Chersich, *CHEMTECH*, (1985)756.

[45] J.Haber, T.Machej and T.Czeppe, *Surf. Sci.*, **151**(1985)301.

[46] Z.C.Kang and Q.X.Bao, *Appl. Catal.*, **26**(1986)251.

[47] J.Kijenski, A.Bailker, M.Glinski, P.Dollenmeier and A.Wokaum, *J. Catal.*, **101**(1986)1.

[48] A.Vejux and P.Courtine, *J. Solid State Chem.*, **63**(1986)173.

[49] G.Busca, G.Centi, L.Marchetti and F.Trifiro, *Langmuir*, **2**(1986)568.

[50] J.Leyer, R.Margraf, E.Taglauer and H.Knözinger, *Surf. Sci.*, **201**(1988)603.

[51] K.Asakura and Y.Iwasawa, *Chem. Lett.*, (1986)859.

[52] K.Asakura and Y.Iwasawa, *Chem. Lett.*, (1988)633.

[53] K.Asakura and Y.Iwasawa, *J. Phys. Chem.*, **95**(1991)1711.

[54] T.Tanaka, H.Nojima, H.Yoshida, H.Nakagawa, T.Funabiki and S.Yoshida, *Catal. Today*, **16**(1993)297.

[55] S.Yoshida, T.Tanaka, T.Hanada, T.Hiraiwa, H.Kanai and

T.Funabiki, *Catal. Lett.*, **12**(1992)277.

[56] J.M.Jehng and I.E.Wachs, *J. Raman Spectroscopy*, **22**(1991)83.

[57] J.M.Jehng and I.E.Wachs, *Prepn. Am. Chem. Soc., Div. Pet. Chem.*, **34**(1989)546.

[58] J.M.Jehng and I.E.Wachs, *J. Phys. Chem.*, **95**(1991)7373.

[59] J.M.Jehng and I.E.Wachs, *J. Mol. Catal.*, **67**(1991)369.

[60] M.A.Vuurman and I.E.Wachs., *J. Phys. Chem.*, **96**(1992)5008.

[61] S.Yoshida, Y.Nishimura, T.Tanaka, H.Kanai and T.Funabiki, *Catal. Today*, **8**(1990)67.

[62] J.M.Jehng and I.E.Wachs, *Chem. Mater.*, **3**(1991)100.

[63] E.I.Ko, R.Bafrali, N.T.Nuhfer and N.J.Wagner, *J. Catal.*, **95**(1985)260.

[64] E.I.Ko and J.G.Weissman, *Catal. Today*, **8**(1990)27.

[65] S.Denofre, Y.Gushikem, S.C.Castro and Y.Kawano, *J. Chem. Soc., Faraday Trans.*, **89**(1993)1057.

[66] M.Nishimura, K.Asakura and Y.Iwasawa, *J. Chem. Soc., Chem. Commun.*, (1986)1660.

[67] M.Nishimura, K.Asakura and Y.Iwasawa, *Chem. Lett.*, (1987)573.

[68] M.Nishimura, K.Asakura and Y.Iwasawa, *Proc. 9th Inter. Congr. Catal.*, **IV**(1988)1842.

[69] P.A.Burke and E.I.Ko, *J. Catal.*, **129**(1991)38.

[70] M.Shirai, N.Ichikuni, K.Asakura and Y.Iwasawa, *Catal. Today*, **8**(1990)57.

[71] J.Datka, A.M.Turek, J.M.Jehng and I.E.Wachs, *J. Catal.*, **135**(1992)186.

[72] K.Tanabe, *Solid Acids and Bases*, Academic Press, New York, 1970.

[73] H.A.Benesi and B.H.C.Winquist, *Adv. Catal.*, **27**(1978)97.

[74] Y.Inoue, H.Yamazaki and Y.Kimura, *Bull. Chem. Soc. Jpn.*, **58**(1985)2481.

[75] G.Connel and J.A.Dumesic, *J. Catal.*, **102**(1986)216.

[76] G.Connel and J.A.Dumesic, *J. Catal.*, **105**(1987)285.

[77] A.M.Turek, I.E.Wachs and E.DeCanio, *J. Phys. Chem.*, **96**(1992)5000.

[78] J.M.Jehng and I.E.Wachs, *Catal. Today*, **16**(1993)417.

[79] Y.Iwasawa, *Res. Chem. Intermed.*, **15**(1991)183.

[80] Z.Dawoodi, M.L.H.Green, V.S.B.Mtetwa and K.Prout, *J. Chem. Soc., Chem. Commun.*, (1982)802.

[81] N.Koga, S.Obara, K.Kitaura and K.Morokuma, *J. Am. Chem. Soc.*, **107**(1985)7109.

[82] Y.Iwasawa, Y.Nakano and S.Ogasawara, *J. Chem. Soc., Faraday Trans. 1*, **74**(1978)2968.

[83] M.M.Abouelleil and F.J.Leonberger, *J. Am. Ceram. Soc.*, **72**(1989)1311.

[84] P.V.Lenzo, E.G.Spencer and A.A.Ballman, *Appl. Phys. Lett.*, **11**(1967)23.

[85] H.Kominami, M.Inoue and T.Inui, *Catal. Today*, **16**(1993)309.

[86] H.Rebbah, G.Desgardin and B.Raveau, *Mat. Res. Bull.*, **14**(1979)1125.

[87] S.Kikkawa and M.Koizumi, *Mat. Res. Bull.*, **18**(1989)533.

[88] H.Tagaya, K.Saito, T.Kuwahara, J.Kadokawa and K.Chiba, *Catal. Today*, **16**(1993)463.

[89] J.Gopalakrishinan, V.Bhat and B.Ravau, *Mat. Res. Bull.*, **22**(1987)413.

[90] A.J.Jacobson, J.W.Johnson and J.T.Lewandwski, *Mat. Res. Bull.*, **22**(1987)45.

[91] T.Matsuda, T.Fujita and N.Miyamae, *Catal. Today*, **16**(1993)455.

[92] E.M.Thorsteinson, T.P.Wilson, F.G.Young and P.H.Kasai, *J. Catal.*, **52**(1978)116.

[93] O.Desponds, R.L.Keiski and G.A.Somorjai, *Catal. Lett.*, **19**(1993)17.

[94] R.H.H.Smits, K.Seshan, H.Leemreize and J.R.H.Ross, *Catal. Today*, **16**(1993)513.

[95] K.Tanabe, M.Misono, Y.Ono and H.Hattori, *New Solid Acids and Bases*, Kodansha, Tokyo, 1979.

[96] Y.C.Kim, W.Ueda and Y.Moro-oka, *Appl. Catal.*, **70**(1991)189.

[97] I.Matsuura, H.Oda and K.Oshida, *Catal. Today*, **16**(1993)547.

[98] for example, S.J.Tauster, S.C.Fung, R.T.K.Baker and J.A.Horsley, *Science*, **211**(1981)1121; S.J.Tauster, *Acc. Chem. Res.*, **20**(1987)389; R.Burch, *Hydrogen Effects in Catalysis*, Dekker, New York, 1988.

[99] G.L.Haller and D.E.Resasco, *Adv. Catal.*, **36**(1989)173.

[100] articles in: B.Imerik et al. (eds.), *Metal-Support and Metal-Additive Effects in Catalysis*, Elsevier, Amsterdam, 1986.

[101] E.I.Ko, J.M.Hupp, F.H.Rogan and N.J.Wagner, *J. Catal.*, **84**(1983)85.

[102] E.I.Ko, S.Winston and C.Woo, *J. Chem. Soc., Chem. Commun.*, (1982)740.

[103] K.Kunimori, H.Abe, E.Yamaguchi, S.Matsui and T.Uchijima, *Proc. 8th Inter. Congr. Catal.*, **5**(1984)251.

[104] K.Kunimori, K.Ito, K.Iwai and T.Uchijima, *Chem. Lett.*, (1986)573.

[105] K.Kunimori, Z.Hu, A.Maeda, H.Nakamura and T.Uchijima, *Int. Conf. Surface Colloid Sci. 6th*, (1988).

[106] K.Kunimori, Z.Hu, T.Uchijima, K.Asakura, Y.Iwasawa and M.Soma, *Catal. Today*, **8**(1990)85.

[107] M.M.Pereira, F.B.Noronha and M.Schmal, *Catal. Today*,

16(1993)407.

[108] A.Maeda, K.Kunimori and T.Uchijima, *Nippon Kagaku Kaishi*, (1992)267.

[109] D.A.G.Aranda, F.B.Passos, F.B.Noronha and M.Schmal, *Catal. Today*, **16**(1993)397.

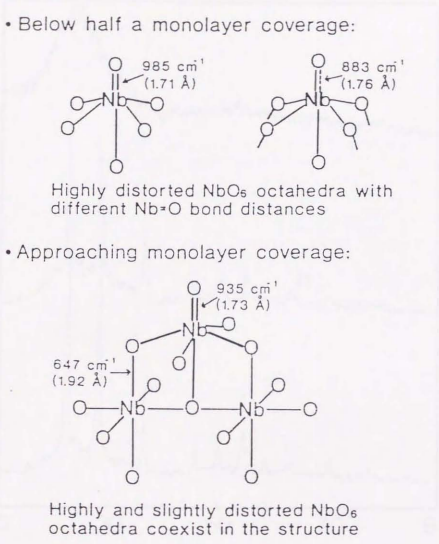

Figure 1. A plausible model for molecular structures of the dehydrated surface niobium oxide species [58].

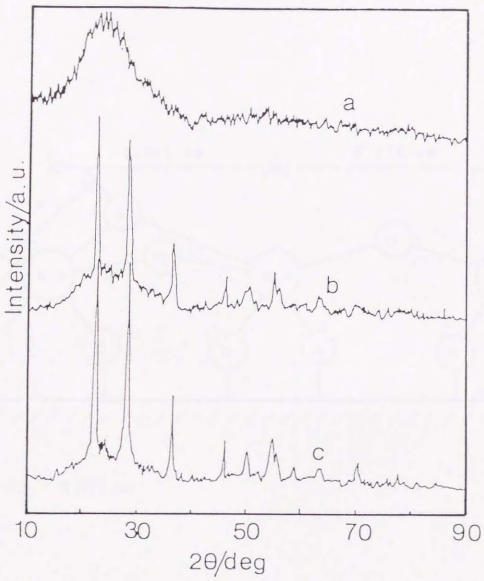

Figure 2. X-ray diffraction patterns for (a)one-atomic-layer niobium oxide, (b)impregnation niobium oxide on SiO_2 from $NbCl_5$, (c)impregnation niobium oxide on SiO_2 from $Nb(OC_2H_5)_5$ [53].

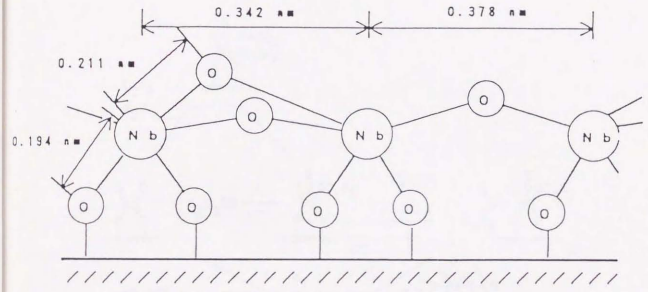

Figure 3. Proposed model structure for the niobium oxide one-atomic-layer on silica [53].

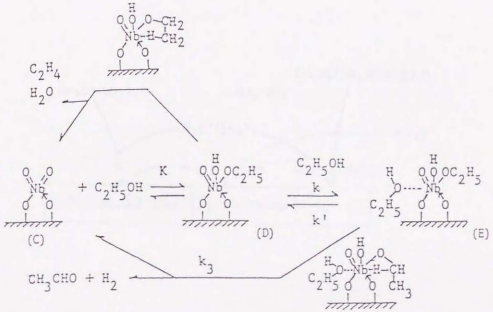

Figure 4. Self-assisted mechanism for ethanol dehydrogenation on the Nb monomers attached on silica [79].

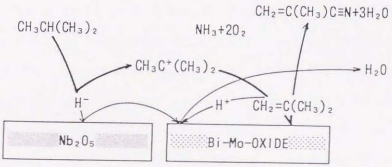

Figure 5. Reaction scheme of methacrylonitrile formation from isobutane ammoxidation on mixed catalyst composed of Bi-Mo-based composite oxide and strong acidic Nb_2O_5 [97].

2. Experimental Section

2.1. Catalyst Preparation

The dimeric Nb complex $[Nb(\eta^5\text{-}C_5H_5)H\text{-}\mu\text{-}(\eta^5,\eta^1\text{-}C_5H_4)]_2$ was synthesized from the reaction of $NbCp_2Cl_2$ (Aldrich) with NaH (Aldrich) in water-free THF in a similar was to that previously reported [1,2]. Cause the complex was sensitive for moisture and air, it was handled and kept under vacuum or high purity Ar gas (99.9999 %, Takachiho Trading Co.Ltd). The silica-attached Nb dimer catalysts were prepared as follows. SiO_2 pretreated at 673 K to control the surface OH density about 2 OH nm^{-1} was immersed in a toluene solution of the dimeric Nb complex to react the complex with the surface OH groups of SiO_2 at 313 K under high purity Ar (99.9999 %), followed by decantation and washing twice by toluene to remove unreacted complex, and by evacuation to remove the residual solvent. After the attachment processes were completed, the samples were reduced with hydrogen at 823 K. The treated samples were slowly exposed to oxygen at room temperature, then oxidized with oxygen at 773 K to convert them to the oxidized form. Four different kinds of SiO_2 (Aerosil 200, Aerosil 300, Fuji-Davison micro bead silica gel 4B and Aerosil Ox. 50) were used as support with the surface area of 200, 300, 500 and 50 m^2/g, respectively. The catalysts obtained by using these silicas are designated in chapter 4 and 5 as $Nb_2(1)$, $Nb_2(2)$, $Nb_2(3)$ and $Nb_2(4)$, respectively. Conventional supported Nb catalysts for the identical silicas were also prepared by a usual impregnation method using a methanol solution of $NbCl_5$, followed by dry at 373 K and calcination at 773 K in air. Nb loadings were regulated to be the values around 1.0 wt%. The catalyst treated in chapter 3 was supported on one type of SiO_2 (Aerosil 200), so the special designation was not used in chapter 3.

2.2. EXAFS/XANES Spectroscopy

The Nb K-edge X-ray absorption spectra at 70 K were obtained in a transmission mode at the EXAFS facilities installed on the BL-10B line of the Photon Factory in National Laboratory for High Energy Physics (KEK-PF) (Proposal No. 88-020). The synchrotron radiation for EXAFS measurements was operated at a ring energy of 2.5 GeV with a storage positron current of 150-250 mA and monochromatized by a channel cut Si(311) crystal. Energy calibration was performed using the Nb foil K-edge inflection point at the edge (18986.9 eV). Ion chambers filled with $Ar+N_2$ (50 % / 50 %) and Ar were used for X-ray detection of I_o (before sample) and I (after sample), respectively.

The glass cell sealed with two Kapton windows was used to measure the X-ray absorption spectra. The cell length was chosen as 20 mm or 10 mm for the total absorption coefficient not to exceed 3. The cell was connected to a pyrex U-shape tube in a closed circulating system in which the catalysts were treated and the catalytic reactions were conducted, so that the sample transfer was performed without contacting air.

The oscillation part of the absorption as a function of the X-ray photon energy was extracted as described elsewhere [3]. Normalization of the EXAFS data was carried out by fitting the background absorption coefficient around the energy region by *ca.* 50 eV higher than the absorption edge with the smoothed absorption coefficient of an isolated atom (Victoreen equation, $C_o\lambda^3+D_o\lambda^4$).

Fourier transformation (FT) of k^3-weighted normalized EXAFS data was performed over the 30-130 nm^{-1} range except the 30-120 nm^{-1} range for the $Nb_2(1)$, to obtain the radial distribution function. The Fourier-filtered data were analyzed by use of the

least-square curve fitting method with eqn (1), (2) [3,4].

$$\chi(k)=\Sigma N_j F_j(k)\exp(-2\sigma_j^2 k^2)\sin(2kr_j+\phi_j(k))/kr_j^2 \quad (1)$$

$$k_j=(k^2-2m_e\Delta E_{oj}/\hbar^2)^{1/2} \quad (2)$$

where N_j, r_j, σ_j, ΔE_{oj} and m_e represent the coordination number, bond distance, Debye-Waller factor, the difference between the model compound and experimental threshold energies and the mass of electron, respectively. F_j and ϕ_j are amplitude and phase shift functions, respectively. Precise structural characterization of surface species with EXAFS requires the use of reference materials in the experimentation and data analysis [5]. Then the curve fitting analysis was performed by using empirical parameters extracted from $NbCp_2Cl_2$, Nb foil, $LaNbO_4$ and $NbSi_2$ for Nb-C, Nb-Nb, Nb-O and Nb-Si bonds, respectively. Since the length of Nb-C in the $NbCp_2Cl_2$ is close to that of Nb-Cl [6] as listed in Table 1, the contribution of Nb-Cl was subtracted by use of Nb-Cl bond extracted from $NbCl_5$. The coordination numbers and bond distances used for model parameters as above mentioned are listed in Table 2. The error of curve fitting analysis was estimated by using Rf represented in eqn (3).

$$R_f=\int|k^3\chi(k)^{obs}-k^3\chi(k)^{calc}|^2dk/\int|k^3\chi(k)^{obs}|^2dk \quad (3).$$

Data analyses were performed using Program EXAFS2N with the HITAC M-682H computer system at the University of Tokyo.

2.3. Catalytic Reaction of Ethanol

Catalytic ethanol dehydration reactions were carried out in a closed circulating system equipped with a gas chromatograph (Shimadzu GC-8A). The amount of the catalyst was *ca.* 0.2 g for a typical reaction. The catalyst was treated with 13.3 kPa of oxygen at 773 K for 1 h, followed by evacuation at the same temperature for 30 min *in situ* before use as catalyst. Ethanol (Wako Pure Chemical Co., Ltd.) was purified by freeze-thaw cycles before use. Reaction products were separated by a 2 m DOS column (Gasukuro Kogyo Inc.) at 338 K and detected by TCD.

References

[1] L.J.Guggenberger and F.N.Tebbe, *J. Am. Chem. Soc.*, **93**(1971)5924.

[2] D.A.Lemenovskii, I.F.Urazowskii, I.E.Nifant'ev and E.G.Pervalova, *J. Organomet. Chem.*, **292**(1985)217.

[3] K.Asakura and Y.Iwasawa, *J. Chem. Soc., Faraday Trans. 1*, **84**(1988)2445.

[4] B.K.Teo, *EXAFS: Basic Principles and Data Analysis, Inorganic Concepts*, Vol. 9, Springer, Berlin, 1986.

[5] D.C.Koningsberger and R.Prins (eds.), *X-ray Absorption: Principles and Applications, Techniques of EXAFS, SEXAFS and XANES*, J. Wiley, New York, 1988.

[6] K.Prout, T.S.Cameron, R.A.Forder, S.R.Critchley, B.Denton and G.V.Rees, *Acta. Cryst.*, **B30**(1974)2290.

Table 1. Bond distances of $NbCp_2Cl_2$ [6]

bond	bond length / nm
Nb-C(1)	0.240
Nb-C(2)	0.238
Nb-C(3)	0.241
Nb-C(4)	0.244
Nb-C(5)	0.239
Nb-C(6)	0.237
Nb-C(7)	0.239
Nb-C(8)	0.237
Nb-C(9)	0.237
Nb-C(10)	0.240
Nb-Cl(1)	0.2464
Nb-Cl(2)	0.2475

mean distance for Nb-C: 0.2392,

meas distance for Nb-Cl: 0.247.

Table 2. Coordination numbers and bond distances for model compounds

bond	model compound	C.N.[a]	r[b] / nm
Nb-O	$LaNbO_4$	4	0.1899
Nb-Nb	Nb foil	8	0.2858
Nb-Si	$NbSi_2$	8	0.26852
Nb-C	$NbCp_2Cl_2$[c]	10	0.2392

a: coordination number, b: bond distance, c: Nb-Cl contribution was subtracted (see text).

3. Design of Nb dimers on SiO_2: Regulation of Acidity-Basicity by the number of Metal Atoms in Surface Active Sites

3.1. Introduction

Advances in surface synthesis by surface organometallic technique and characterization by EXAFS spectroscopy are leading to a rapid progress in design of solid catalyst surfaces [1-5]. Observation and control of behaviors of atoms or molecules in active sites are important for molecular-level developments of catalyst preparations as well as for understanding essential factors of the genesis of solid catalysis.

The SiO_2-attached Nb monomer shown in Figure 1(A) has been found to be the first active Nb sample for the catalytic dehydrogenation of ethanol [6,7]. Ethanol adsorbs on Nb=O to form OH and C_2H_5O groups, but the species (B) in Figure 1 was very stable in vacuum and decomposed to ethene and water only above 600 K. However, in the presence of the second ethanol, the Nb-ethoxide depicted in Figure 1(C) is decomposed even at 400 K, where the switchover of reaction path from dehydration to dehydrogenation is observed (self-assisted dehydrogenation mechanism) [7]. Similar observations about the adsorbate-intermediate interaction leading to catalytic cycles (reactant-promoted mechanism) have been reported for water gas shift reaction [8,9].

The aim of this study is (1) to regulate the catalysis by molecular design of reaction sites, (2) to find the effect of the second Nb atom instead of the second ethanol molecule in species (C) depicted in Figure 1, and (3) to understand the cooperative catalysis of two adjacent Nb atoms as a model for general metal oxide catalysts. In this chapter I reports the preparation of new Nb-dimers attached on SiO_2 (Aerosil 200) and the first example of the change in acid/base catalytic properties by the

nucleation of one Nb atom to two Nb atoms in active structures. The mechanism characteristic of the dimer structure, influencing the rate constants for intra- and inter-molecular dehydration of ethanol, is also discussed.

3.2. Results and Discussion

3.2.1. Structure of Nb dimers on SiO_2

Figure 2 shows the preparation steps and structures for Nb dimers attached on SiO_2 (Aerosil 200). The dinuclear complex (1) reacted with surface OH groups of SiO_2 at 313 K as proved by the decrease of the ν(OH) (3743 cm^{-1}) intensity. Upon the interaction, 0.8-0.9 H per Nb atom were evolved (Table 1). The value is less than quantitative amount because the quantitative detection of H_2 evolved during the reaction of (1) with oxides in organic solvents is generally difficult. The IR and MS data reveal that each H ligand of (1) reacted with one (not two) OH group to form (2) as shown in Figure 2. The TD spectra in Figure 3 show twin peaks at 480 K and 570 K for cyclopentadiene with a nearly 1:1 ratio (total amount= 1.93-2.0 per Nb in Table 1). Similar TD spectra of 0.1 and 1.0 wt% samples in Figure 3 suggest almost uniform distribution of Nb species on SiO_2, where two different cyclopentadienyls (η^5-C_5H_5 and η^5,η^1-C_5H_4) are present also in (2) similarly to (1).

Figure 4 shows the k^3-weighted EXAFS oscillation (a) and its associated Fourier transform (b) for (2). The inverse Fourier filtering data were analyzed by a curve fitting technique in Figure 4(c). The best-fit results are listed in Table 2. The observation of Nb-Nb length at 0.334 nm with the coordination number (C.N.) of 0.9(±0.1) demonstrates that the dimeric

structure was maintained on SiO_2. The C.N. of 1.3(±0.2) for Nb-O also support the unidentate Nb structure (2).

The (2) was reduced with H_2 at 823 K to (3), which was oxidized with O_2 at 773 K to Nb^{5+} level characterized by uptaking the quantitative amount of O_2 in Table 1. The O_2 uptake was determined by taking account of small amounts of CO_2 formed by oxidation of the residual carbons in (3). Figure 5 shows the EXAFS data of (4). The first peak in the Fourier transform (b) should be due to Nb-O bond, but the analyses based on one-wave fitting (Nb-O) and two-waves fitting (Nb-O and Nb-O) did not give good fits (curves (d) and (e), showing 7.42 % and 5.09 % of the reliability factor (R_f), respectively). Then, I performed three-waves fitting (Nb-O, Nb-O and Nb-O) in the curve (f) which showed the best-fit result with R_f=3.23 %. The second peak may be due to Nb-Nb and/or Nb-Si. The shoulder at *ca.* 53 nm^{-1} in the oscillation (a) has been attributed to the presence of Nb-Si bond [10,11]. The best-fit result was obtained by two waves of Nb-Nb and Nb-Si. Finally, five-waves fitting analysis (filtering range: 0.10-0.35 nm) was performed in the curve (c) of Figure 5. The best-fit results are listed in Table 2. The observation of Nb-Nb bond at 0.303 nm with C.N. of 0.9(±0.1) demonstrates the retention of a dimeric structure on SiO_2. The Nb-Si length was determined as 0.328 nm with C.N. of 2.3(±0.2). The length is similar to 0.326 nm for the Nb monomer (Figure 1(A)) [7]. There are two different Nb-O bonds at 0.193 nm and 0.213 nm. The former distance is the same as that for Nb-O(surface) in the Nb monomer, and the C.N. of 1.9(±0.2) is the onset of Nb-Si. Thus, the 0.193 nm bond is assigned to the bonding of Nb with two surface oxygen atoms as shown in Figure 2. The bond of 0.179 nm is straightforwardly assigned to Nb=O bond. The remaining Nb-O

bond at 0.213 nm with C.N. of 1.1(±0.1) is due to the oxygen-bridged structure (4) with the Nb-Nb separation of 0.303 nm. The similar bond distances (0.209-0.211 nm) have been reported for Nb-O (bridged) bonds for Nb-oxide monolayers on SiO_2 [12]. The EXAFS spectrum of (4) showed a distinct 1s→4d transition, which implies a tetrahedral/distorted tetrahedral symmetry. The CT band for Nb=O was observed at 227 nm, excluding the possibility of an octahedral symmetry. These results also confirm the structure (4) in Figure 2. The Nb-Nb separation in T- and H-Nb_2O_5 ranges over 0.299-0.389 nm [13]. The Nb-Nb distance in (4) is among these distances, but close to the shortest one, and much shorter than 0.335-0.392 nm for Nb-oxide monolayers on SiO_2 [12]. The value of 0.303 nm is also shorter than 0.311 nm for the dinuclear Nb complex (1) having a direct interaction between two Nb atoms. In the structure (4) Nb-Nb bonding is not drawn because the Nb atom is formally situated in 5+ state, but the character of Nb in (4) may be expected to be different from the isolated Nb monomer (Figure 1(A)).

3.2.2. Regulation of acidity/basicity in catalysis

Ethanol (3.3 kPa) was admitted onto (4) to form $Nb(OH)(OC_2H_5)$ at 373 K followed by evacuation for 30 min (ν(OH): 3471 cm^{-1}, ν(CH): 2979, 2937, 2900 and 2883 cm^{-1}), and the TD spectrum at a heating rate of 4 $Kmin^{-1}$ was taken as shown in Figure 6. Ethene and diethyl ether besides ethanol were desorbed. The peak temperature (610 K) for ethene was lower than 690 K for the Nb monomer represented in Figure 1(B), suggesting the promotion of ethene formation with the dimer (4). Figure 7 shows EXAFS data of (4) after admission of ethanol. The characteristic feature of the EXAFS analysis for the sample

saturated with ethanol at 523 K in Table 3 is the disappearance of the Nb=O bond. The deducement of 1s→4d transition peak in the XANES spectrum also confirmed the vanishment of Nb=O bond. Instead, the C.N. of the Nb-O bond at 0.192 nm increased to 3.9(±0.3) by 2 from 1.9(±0.2) for the catalyst (4), which agrees with the formation of $Nb(OH)(OC_2H_5)$ by the dissociative adsorption of ethanol. The other bonds remained unchanged, demonstrating no change in the oxygen-bridged dimeric structure.

The catalytic dehydration and dehydrogenation of ethanol were carried out in the temperature range 473-573 K. The Nb monomer catalyst exhibited high activity and selectivity for the dehydrogenation to produce acetaldehyde, indicating a basic character of the Nb monomer [6,7]. On the other hand, the Nb dimer catalyst (4) showed a high selectivity for dehydration to form diethyl ether and ethene in Table 4. The dehydrogenation was remarkably suppressed and the dehydration was promoted on the dimers (4) as compared with the monomers. The results imply that the Nb dimers on SiO_2 have an acidic character. The catalytic feature of the Nb dimers was independent of the Nb loadings in the range 0.10-1.6 wt%, suggesting a nearly uniform property of Nb sites on SiO_2 (Table 4), which is in agreement with the structural data by EXAFS. The conventional impregnation Nb catalysts were less active and unselective. It is to be noted that the change of the number of Nb atoms in active sites from one to two metal gave rise to the complete reverse of basicity/acidity in catalytic properties.

3.2.3. Mechanism and change of rate constants

The rate of ethene formation was accelerated 1.7 times by replacing C_2H_5OH by C_2D_5OD as shown in Figure 8. The

substitution of the OH hydrogen with deuterium gave almost no effect on the rate. The inverse isotope effect can be explained by a late transition-state theory. By taking into account the vibrational partition functions, the ratio of the rate constants (k_D/k_H) is expressed by equation (1). I adopted ν(OH) of H_2O and ν(CH) of methylene group as the vibrational modes of the transition state (6), while the observed values were used for the vibrational modes of Nb(OH)(OC_2H_5) (5) as depicted in Figure 9. The calculated inverse isotope effect (k_D/k_H) was 1.6, which is in good agreement with the experimental value.

$$k_D/k_H=\prod\exp[h(\nu_{Hi}^{+}-\nu_{Di}^{+}-\nu_{Hi}+\nu_{Di})/2kT] \quad (1)$$

$$=\exp[hc(\nu_a(H_2O)-\nu_a(D_2O)-\nu(\text{Nb-OH})+\nu(\text{Nb-OD}))/2kT]\cdot$$
$$\exp[hc(\nu_s(H_2O)-\nu_s(D_2O)-\nu_{as}(CH_3)+\nu_{as}(CD_3))/2kT]$$
$$=\exp[hc(3657-2671-3471+2597)/2kT]\cdot$$
$$\exp[hc(3657-2671-2979+2229)/2kT]$$
$$=1.6$$

Ethene is formed by the intramolecular dehydration of species (5) and (7) as shown in Figure 10. The saturation mass of adsorption for ethanol on the dimer (4) was one ethanol per Nb atom under reaction conditions. Using the equilibrium constants (K_1 and K_2) in Figure 10, the amount of ethanol adsorbed (V_{ad}) is expressed by equation (2).

$$V_{ad}=[S_1Et_1]+2[S_0Et_2] \quad (2)$$

$$=[S]_0(K_1P_E+2K_1K_2P_E^2)/2(1+K_1P_E+K_1K_2P_E^2) \quad (3),$$

where P_E and $[S]_0$ represent the partial pressure of ethanol and the number of adsorption sites, respectively. From equation (3)

and the data of the adsorption isotherm, K_1 and K_2 were determined to be $6.0\times10^{-3}Pa^{-1}$ and $2.1\times10^{-3}Pa^{-1}$ at 523 K, respectively.

As the rate of ethene formation (v) is given by equation (4),

$$v=k_2[S_1Et_1]+2k_3[S_oEt_2] \quad (4)$$

the first-order rate constants, k_2 and k_3, for the dehydration of (5) and (7) obtained to be $4.7\times10^{-3}min^{-1}$ and $1.8\times10^{-3}min^{-1}$ at 523 K, respectively. k_2 was about 3 times larger than k_3, which shows that the dehydration of ethanol on a Nb site markedly reduced by the presence of the second ethanol on the adjacent Nb site. It is to be noted that the rate constant is largely affected through the adsorbate-adsorbate/Nb-Nb interaction of the dimer site. Consequently, the rate of ethane formation was deviated downward from the first-order dependency on V_{ad} in Figure 11. Instead, the selectivity to diethyl ether formation increased. The rate of diethyl ether formation (v') was proportional to the square of V_{ad} as shown in Figure 7.

The rate constant (k_1) for diethyl ether formation given by equation (5)

$$v'=k_1[S_oEt_2] \quad (5)$$

was determined to be $8.0\times10^{-3}min^{-1}$ (523 K). The rate constants, k_1-k_3, varied with the Nb-Nb separation. The larger the Nb-Nb separation, the smaller the ratio (k_2/k_3) and the ratio (v'/v) became. This kind of control in the ratio of rate constants and rates was not possible with the conventional impregnation

catalysts.

The insulated character in electronic state of [NbO_4] structure drastically changed when NbO_4 species (A) was attached to SiO_2 surface through oxygen atoms [13]. The band gap becomes small as enough to be 0.30 eV and the component of Nb 4d orbital comes down to the occupied levels to mix with oxygen 2p levels by a DV-Xα MO calculation on the basis of the structures by EXAFS. Thus, the electron density of Nb 4d orbitals for the attached Nb monomer (A) increases to some extent by Mulliken population charge analysis. The Nb dimer (4) also electronically interacts with SiO_2 surface. The charge population on Nb in the dimer (4) reduced to 92 % of that of the monomer (A), while that of the bridged oxygen increased by 9 % as compared with that of the oxygen atom without adjacent Nb atom as shown in Figure 12. This trend leads to an increase in acidic character of Nb site. The adjacent Nb atom in the dimer (4) may also change the local conformation of Nb sites. In the dimer structure (4) the access of a second ethanol molecule to the Nb atom with a first ethanol molecule in a preferable conformation is difficult unlike to the case of the monomer (C). In other words, the assisted-dehydrogenation [7] is not possible with the dimer (4).

3.3. Conclusions

(1) New Nb dimers on a SiO_2 surface prepared by using [Nb(η^5-C_5H_5)H-μ-(η^5,η^1-C_5H_4)]$_2$ were found to have an oxygen-bridged dimeric structure (Nb-O(surface)=0.193 nm; Nb--Si=0.328 nm; Nb--Nb=0.303 nm) by EXAFS. The attached Nb dimers were active for ethanol dehydration in contrast to the dehydrogenation ability of the Nb monomer catalyst.

(2) The regulation of the catalysis from dehydrogenation to dehydration, or equivalently from basic property to acidic property, was achieved by the nucleation of one Nb atom to two Nb atoms in active structures. This was due to (i) electronic effect as Nb in the dimer is more Lewis acidic than Nb in the monomer and (ii) geometric effect as the existence of second NbO_4 unit and bridged oxygen in the Nb dimer inhibits the self-assisted dehydrogenation mechanism.

(3) The inverse isotope effect for ethene formation through the late-transition state of reaction was observed.

(4) The rate constant for ethene formation reduced by the second ethanol adsorption on the adjacent Nb site.

References

[1] Y.Iwasawa, *Adv. Catal.*, **35**(1987)187.

[2] Y.Iwasawa(ed.), *Tailored Metal Catalysts*, Reidel, Dortrecht, 1986.

[3] Y.Iwasawa, K.Asakura, H.Ishii and H.Kuroda, *Z. Phys. Chem. N. F.*, **144**(1985)105.

[4] B.C.Gates, L.Guczi and H.Knözinger(eds.), *Metal Clusters in Catalysis, Stud. Surf. Sci. Catal.*, Vol. 29, Elsevier, Amsterdam, 1983.

[5] Y.I.Yermakov, B.N.Kuznetsov and V.A.Zakharov, *Catalysis by Supported Complexes*, Elsevier, Amsterdam, 1981.

[6] M.Nishimura, K.Asakura and Y.Iwasawa, *J. Chem. Soc., Chem. Commun.*, (1986)1660.

[7] M.Nishimura, K.Asakura and Y.Iwasawa, *Proc. 9th Int. Congr. Catal.*, IV(1988)1842.

[8] T.Shido, K.Asakura and Y.Iwasawa, *J. Catal.*, **122**(1990)55.

[9] T.Shido and Y.Iwasawa, *J. Catal.*, **129**(1991)343.

[10] K.Asakura and Y.Iwasawa, *Chem. Lett.*, (1986)859.

[11] K.Asakura and Y.Iwasawa, *Chem. Lett.*, (1988)633.

[12] K.Asakura and Y.Iwasawa, *J. Phys. Chem.*, **95**(1991)1711.

[13] Y.Iwasawa, *Res. Chem. Intermed.*, **15**(1991)183.

Table 1. Characterization of the Nb species (2)-(4)

Nb content on support/wt%	0.1	0.37	1.0	1.6
Amount of H_2 evolved per Nb	0.4	0.4	0.45	0.45
Number of Cp ligands* per Nb	1.93	2.0	2.0	1.98
Consumption of O_2 per Nb (3→4)	0.75	0.71	0.73	0.75
CT bands of (4)/nm	——	227	227	227

*η^5-C_5H_5 and η^5,η^1-C_5H_4 ligands.

Table 2. Curve fitting results for the EXAFS data of (2) and (4)[a]

Species	Bond	C.N.	r/nm[b]	DW/nm[c]
	Nb-O	1.3±0.2	0.201	0.005
(2)	Nb-C	10.0±1.5	0.243	0.008
	Nb-Nb	0.9±0.1	0.334	0.005
	Nb=O	0.6±0.2	0.179	0.008
	Nb-O	1.9±0.2	0.193	0.005
(4)	Nb-O	1.1±0.1	0.213	0.005
	Nb-Nb	0.9±0.1	0.303	0.006
	Nb-Si	2.3±0.2	0.328	0.004

a: 1.0wt%-Nb, b: distance(±0.003 nm), c: Debye-Waller factor, Filtering range: 0.13-0.35 nm (2) and 0.10-0.35 nm (4).

Table 3. Curve fitting results for the EXAFS data of (4)[a] after ethanol adsorption

Bond	C.N.	r/nm[b]	DW/nm
Nb-O	3.9±0.3	0.192	0.008
Nb-O	1.1±0.1	0.213	0.004
Nb-Nb	1.1±0.1	0.304	0.006
Nb-Si	2.3±0.2	0.328	0.004

a: 1.0 wt%-Nb, b: ±0.003 nm.

Table 4. Typical results for activities and selectivities of three different Nb catalystsin the dehydration and dehydrogenation of ethanol

Cat.*	React. temp./K	Initial rate** (i)	(ii)	Selectivity/% Ethene	Diethyl ether	Acetaldehyde
(A)	523	1.20	0.05	2.8	1.1	96.1
	548	1.55	0.11	6.1	0.7	93.2
Activation energy/kJ mol^{-1}				——	——	65
(4)						
0.1 wt%	523	0.01	0.19	34.7	61.9	3.4
0.37 wt%	523	0.01	0.17	32.6	63.9	3.5
	548	0.01	1.10	58.1	40.2	1.8
1.0 wt%	523	0.01	0.19	34.2	62.0	3.8
Activation energy/kJ mol^{-1}				119	79	68
Impreg. Catal						
0.45 wt%	523	0.05	0.12	26.0	45.3	28.6
0.92 wt%	523	0.01	0.08	27.2	59.8	13.0
Activation energy/kJ mol^{-1}				129	85	70

* (A): Nb monomer/SiO_2 (2.0 wt%), (4):Nb dimer/SiO_2.

** EtOH: 3.3 kPa, mmolmin^{-1}g-Nb^{-1}, (i)dehydrogenation, (ii) dehydration.

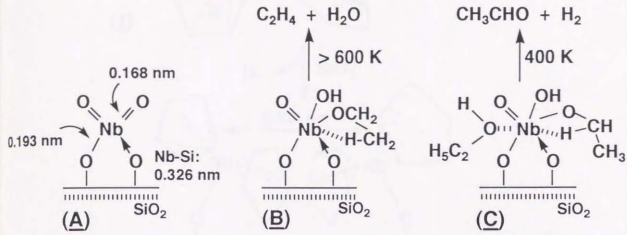

Figure 1. Structures of attached Nb monomer catalysts, (A)oxidized form, (B)one ethanol adsorbed, (C)intermediate for self-assisted dehydrogenation mechanism.

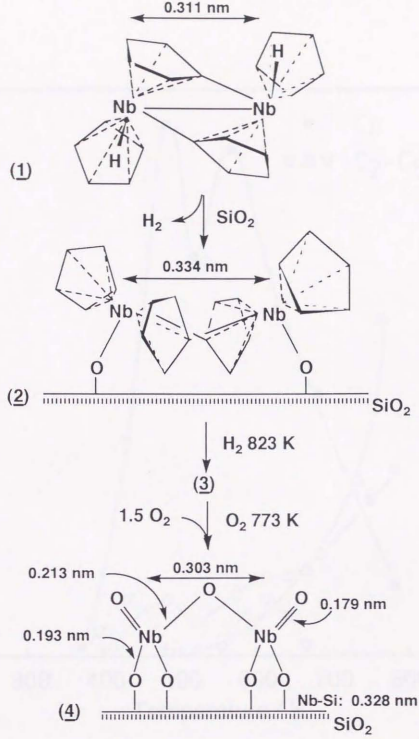

Figure 2. Preparation steps and structures for Nb dimers attached on SiO_2.

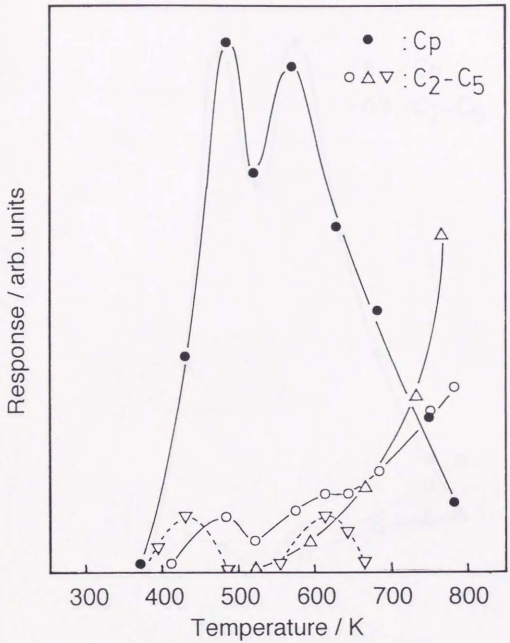

Figure 3(A). TD spectrum of species (2) (0.1 wt%) in the presence of hydrogen (13.3 kPa).

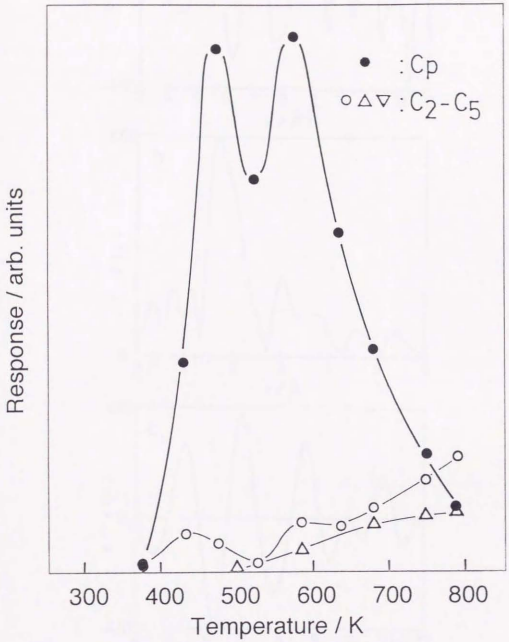

Figure 3(B). TD spectrum of species (2) (1.0 wt%) in the presence of hydrogen (13.3 kPa).

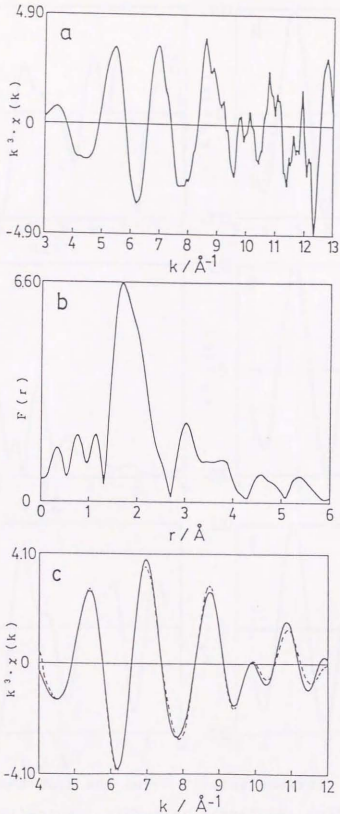

Figure 4. EXAFS data and curve fitting analysis for (2); (a)k^3-weighted oscillation, (b)Fourier transform, (c)curve fitting (solid line: obs., broken line: calc.).

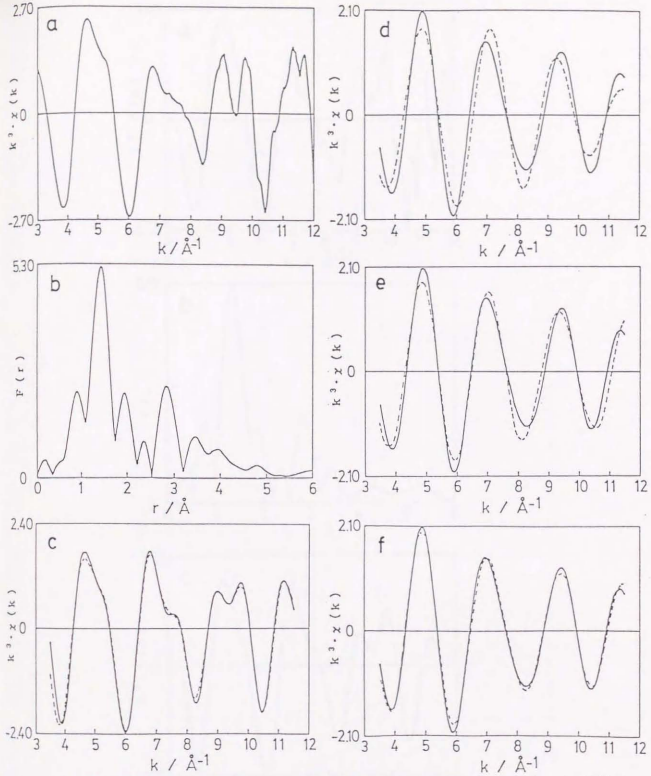

Figure 5. EXAFS data and curve fitting analysis for (4); (a)k^3-weighted oscillation, (b)Fourier transform, (c)five-waves fitting, (d)one-wave fitting (Nb-O), (e)two-waves fitting (Nb-O, Nb-O), (f)three-waves fitting (Nb-O, Nb-O, Nb-O); (solid line: obs., broken line: calc.).

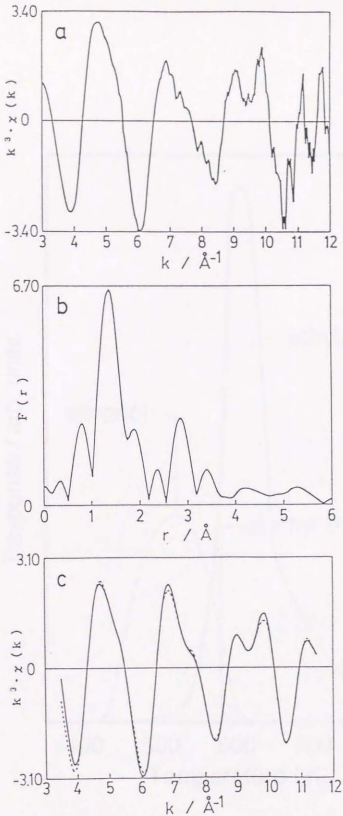

Figure 6. EXAFS data and curve fitting analysis for (4) after ethanol adsorption; (a)k^3-weighted oscillation, (b)Fourier transform, (c)curve fitting (solid line: obs., broken line: calc.).

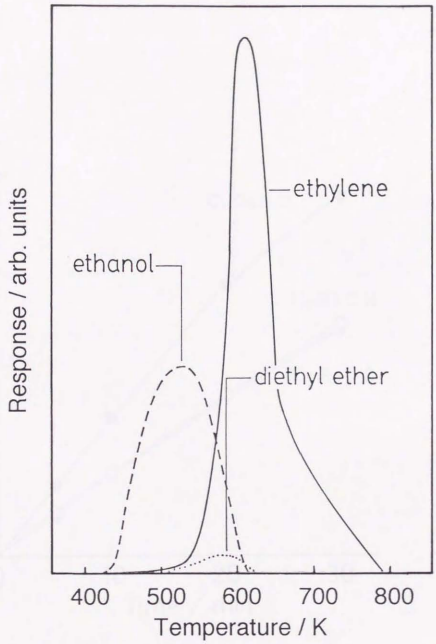

Figure 7. TPD spectrum for (4) after ethanol adsorption.

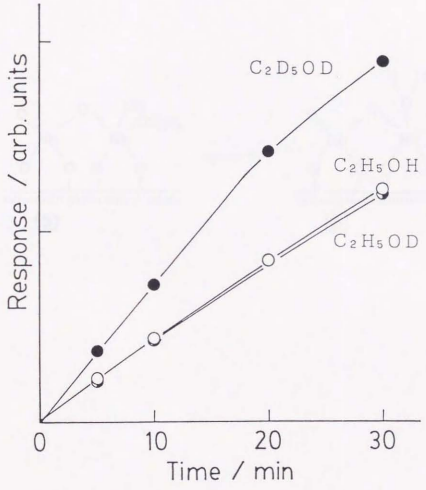

Figure 8. Inverse isotope effect: Ethene formation by the dehydration of C_2H_5OH, C_2H_5OD and C_2D_5OD (3.3 kPa) at 523 K; 1.0 wt%-Nb.

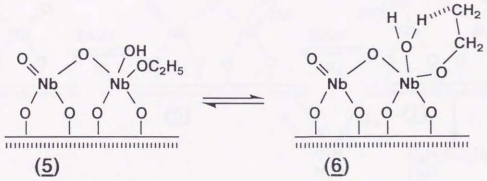

Figure 9. Scheme for inverse isotope effect of ethene formation.

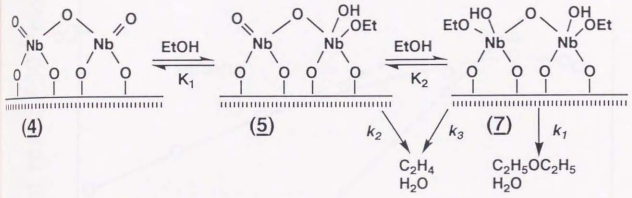

Figure 10. Scheme for ethanol dehydration on Nb dimer catalyst.

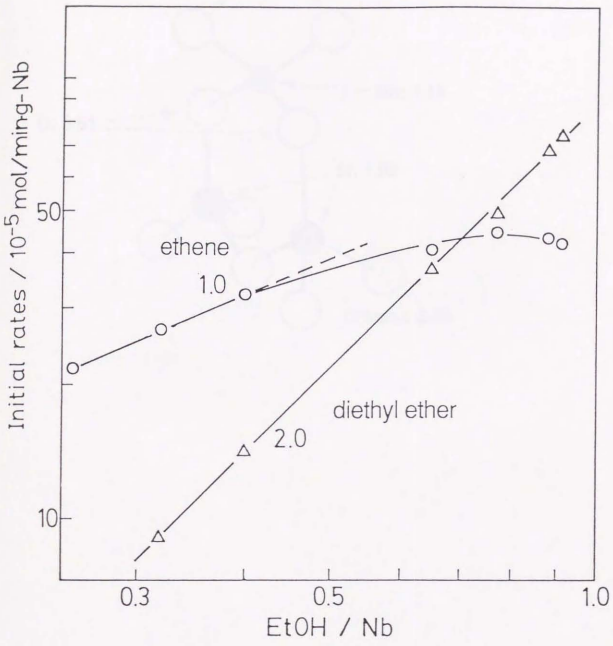

Figure 11. The variation of the initial rates of ethene and diethyl ether formations with EtOH/Nb.

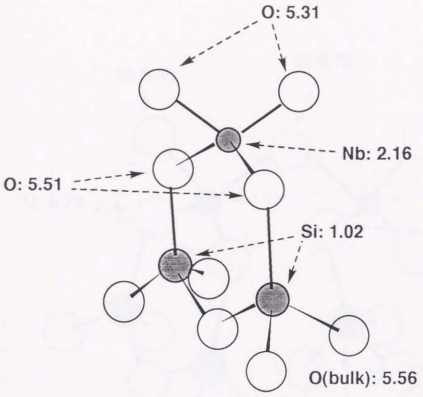

Figure 12(a). Electron densities obtained by Mulliken population analysis for the silica attached Nb monomer catalyst; Nb: 4d orbital, O: 2p orbital, Si: 3p orbital.

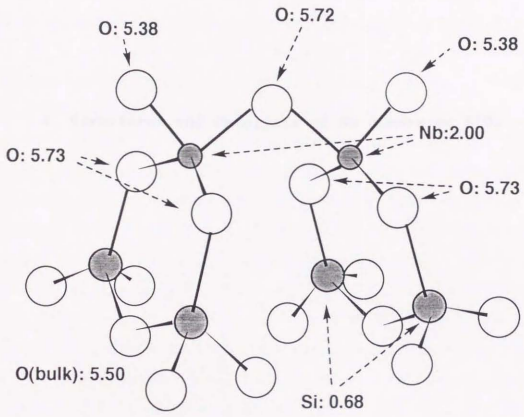

Figure 12(b). Electron densities obtained by Mulliken population analysis for the silica attached Nb dimer catalyst; Nb: 4d orbital, O: 2p orbital, Si: 3p orbital.

4. Structures and Catalysis of Nb dimers on SiO_2

4.1. Introduction

The attached metal catalysts which are prepared by reactions between organometallic compounds and inorganic oxides, followed by suitable chemical treatments depending on what surface active structures should be created, provide basic information on the genesis of solid catalysis and a new way of the developments of catalytic systems [1-5]. Nb monomers on SiO_2 have been demonstrated to be the first active Nb sample for catalytic ethanol dehydrogenation [6,7]. In contrast, the Nb dimers on SiO_2 prepared by using $[Nb(\eta^5\text{-}C_5H_5)H\text{-}\mu\text{-}(\eta^5,\eta^1\text{-}C_5H_4)]_2$ as a precursor were found to show dehydration catalysis, where the change in acid/base catalytic properties by the nucleation of active sites from one Nb atom to two Nb atoms was observed for the first time [8-10]. On the Nb dimer catalysts ethene (ET) formation reduced and diethyl ether (DE) formation was enhanced when two ethanol molecules adsorbed on the two adjacent Nb atoms in a Nb-dimer. Adsorption of ethanol on the Nb dimer catalyst was accompanied with the formation of Nb-OH (ν_{OH}: 3471 cm^{-1}) and Nb-OC_2H_5 (ν_{CH}: 2979, 2937, 2900 and 2883 cm^{-1}), DE was formed by inter-adsorbate dehydration of two ethoxyls on each Nb atom in the dimer and ET was formed by intra-adsorbate dehydration [9].

The present investigation was aimed to (1)preparation of Nb dimer catalysts possessing various Nb-Nb distances, (2)control of intra- and inter-adsorbate dehydration, particularly the regulation of the rate constants and (3)observation of dynamic aspect of dehydration mechanism. For the purpose of (1), four kinds of silicas with various surface areas were uses as support. This chapter reports the structures of new Nb dimer catalysts, the influence of Nb structures to the intra- and inter-molecular

dehydration of ethanol and the outlook for structural change in dimer sites during ethanol dehydration.

4.2. Results and Discussion

4.2.1. Structures of Nb dimers on SiO_2

Figure 1 shows the k^3-weighted Nb K-edge EXAFS oscillations (a) and their associated Fourier transforms (b) for the four Nb dimer catalysts Nb_2(1) (A), Nb_2(2) (B), Nb_2(3) (C) and Nb_2(4) (D). The shoulder at around 53 nm^{-1} in the oscillation has been demonstrated to be due to Nb-Si bond [11-14]. Since all catalysts exhibited the shoulder at *ca.* 53 nm^{-1}, they seem to be chemically attached to SiO_2 surfaces. The chemically attaching reaction of the dimeric Nb precursor with the OH groups of SiO_2 surface was also evidenced by the evolution of H_2 upon supporting and by the decrease in the intensity of ν_{OH} peak [9]. The doublet feature at 90-100 nm^{-1} in the $k^3\chi(k)$ in Figure 1(a) can also be used as a finger print for the existence of Nb-Nb bond in the Nb-SiO_2 systems. The feature was observed for Nb_2(1), Nb_2(2) and Nb_2(4), but not for Nb_2(3), suggesting that there is no Nb-Nb interaction in Nb_2(3).

In order to obtain definite structural information around Nb atom in the attached Nb species, we performed the inverse Fourier transformation and its curve fitting by using the empirical parameters. Curve fitting analyses for Nb_2(1) were performed as follows. The first peak at around 0.15 nm in the Fourier transform (Figure 1(A) (b)) is straightforwardly assigned to Nb-O bond, but the analysis by one-wave fitting (Nb-O) did never fit the observed curve as shown in Figure 2(a). Next we tried the two-waves fitting (Nb-O and Nb-O), resulting in some improvement,

but the amplitude and interval of oscillation was still not reproduced as shown in Figure 2(b). Then, we performed the three-waves analysis (Nb-O, Nb-O and Nb-O) and obtained the best-fitting in Figure 2(c). The second peak at around 0.28 nm in Figure 1(A) (b) may be due to Nb-Nb bond and/or Nb-Si bond [9,12,13]. The one-wave analysis (Nb-Nb) did not agree with the observed oscillation (Figure 2(d)), where there existed the difference between calculated and observed curves both in lower and higher k regions. Moreover, R_f (R-factor) was as large as 9.6 %. As suggested by the shoulder at around 53 nm^{-1} as a fingerprint for Nb-Si bond, then, we tried the two-waves analysis (Nb-Nb and Nb-Si) in Figure 2(e), which shows a good fitting with R_f of 3.6 %. Finally, the five-waves analysis on the basis of three-waves for the first peak and the two-waves for the second peak was performed over the whole range of two peaks in the Fourier transform as shown in Figure 5(A). The best-fit result is listed in Table 1. The coordination number of 0.6, nearly equal to one, for the bond at 0.179 nm means that there is one Nb=O double bond around Nb atom. The Nb-O bond at 0.193 nm showed the coordination number of *ca.* 2 which is close to that of Nb-Si bond (2.3) at 0.328 nm. The 0.193-nm bond length is similar to that of Nb-O bonds chemically attached to SiO_2 surface [6.7]. These indicate that the Nb atoms are bonded to the SiO_2 surface through the Nb-O bond at 0.193 nm in a bidentate form as illustrated in Figure 7. The length of the longest Nb-O bond (0.213 nm) is nearly equal to Nb-bridge-O bond on Nb_2O_5-monolayers on SiO_2 [10,11,13]. Moreover, the fact that the coordination number of the 0.213-nm bond is 1.1 appears to be related to Nb-Nb bonding (0.9). Thus, we assigned the longest Nb-O bond to be due to the Nb-O-Nb bridge-bond which keeps the

dimeric structure as shown in Figure 7.

The profiles of the oscillation and Fourier transform for $Nb_2(2)$ were similar to those of $Nb_2(1)$ as shown in Figure 1(B). Accordingly, the curve fitting analyses for $Nb_2(2)$ were performed in a similar procedure to the case of $Nb_2(1)$. The results of the curve fitting for $Nb_2(2)$ are shown in Figure 5(B). The determined bond distances and coordination numbers for $Nb_2(2)$ in Table 1 essentially resemble those for $Nb_2(1)$. The lengths of Nb-Nb bond (0.308 nm) and Nb-O(bridge) bond (0.218 nm) for $Nb_2(2)$ are longer by 0.005 nm than those for $Nb_2(1)$. The $Nb_2(2)$ structure is illustrated in Figure 7.

Also in the case of $Nb_2(3)$, the first peak at around 0.15 nm in the Fourier transform (Figure 1(C)) straightforwardly assigned to Nb-O bond was analyzed in a similar way to the case of $Nb_2(1)$ and $Nb_2(2)$. The one-wave fitting (Nb-O) was carried out in Figure 3(a), but the calculated curve did not reproduce the observed one. Next, we tried the two-waves fitting (Nb-O and Nb-O). The fitting became much better, but the addition of the third Nb-O bond well reproduced the experimental curve as shown in Figure 3(c). Although the second peak at around 0.3 nm in the Fourier transform (Figure 1(C) (b)) is relatively small, the curve fitting analysis for this peak was performed by assuming Nb-Nb bond in Figure 3(d) because the dimer complex was used as a precursor for the catalyst. The calculated curve was much different from the observed curve particularly in the lower and higher k regions as shown in Figure 3(d) (R_f: 9.3 %). Alternatively, the one-wave fitting by assuming Nb-Si bond was performed because of the existence of the shoulder around 53 nm^{-1} in the oscillation (Figure 1(C) (b)) which suggests the presence of Nb-Si bond [11,12]. The calculated curve reproduced the

experimental one with R_f of 4.1 % (Figure 3(e)). When the Nb-Nb bond was added to the analysis, the R_f was not improved (3.5 %) and the coordination number of added Nb-Nb bond was estimated to be smaller than 0.1. Furthermore, the doublet feature in the oscillation of Figure 1(C) (a) was not observed unlike those for Nb_2(**1**) and Nb_2(**2**). Thus, there is no evidence on the existence of Nb-Nb bonding in Nb_2(**3**) structure. Finally, the four-waves fitting (Nb-O, Nb-O, Nb-O and Nb-Si) was achieved over the whole range of two peaks in the Fourier transform as shown in Figure 5(C). The experimental oscillation was nearly completely reproduced by this fitting analysis. The best-fit result is listed in Table 1. The coordination number of Nb=O bond (0.173 nm) demonstrates that there is one Nb=O double bond around Nb atom. The coordination numbers of Nb-O bond (0.197 nm) and Nb-O bond (0.228 nm) were determined as 2.6 and 0.7, respectively. The sum of the coordination numbers for two bonds is approximately 3, suggesting that Nb atoms are located on the three-fold sites of SiO_2 surface in a terdentate form. The Nb-Si bond has been observed with the Nb/SiO_2 systems with the Nb-O(surface) bond shorter than 0.2 nm [7,9,10-14]. It is therefore supposed that the Nb-Si bond was not observed for the longer Nb-O bond at 0.228 nm. From these results the Nb2(3) structure is pictured in Figure 7.

In the case of Nb_2(**4**), a definite peak around 0.35 nm in the Fourier transform of Figure 1(D) (b) appeared besides the peak at *ca.* 0.30 nm. The 0.28-0.38 nm range was Fourier-filtered to the k-space oscillation in Figure 4(a). The obtained experimental curve was fitted by assuming one-shell (Nb-Nb)(a) and two-shells (Nb-Nb and Nb-Nb)(b). The two-waves fitting analysis was successfully performed in the higher wave-number region in Figure

4(b). Since the shoulder at *ca.* 53 nm^{-1} in the $k^3\chi(k)$ of Figure 1(D) (a) was observed, next, we performed the three-waves fitting (Nb-Nb, Nb-Nb and Nb-Si), which reproduced the observed curve nearly completely (Figure 4(c)). For the analysis of the first peak in the Fourier transform (Figure 1(D) (b)), we have not able to find the Nb=O double bond unlike the other Nb structures. Finally, the five-waves fitting (Nb-O, Nb-O, Nb-Nb, Nb-Nb and Nb-Si) was applied to the range of 0.10-0.38 nm in the Fourier transform as shown in Figure 5(D). The best-fit result islisted in Table 1. From the comparison with the data for $Nb_2(1)$ and $Nb_2(2)$, the Nb atoms in $Nb_2(4)$ are suggested to attach the SiO_2 surface in a bidentate form through Nb-O bond at 0.190 nm (coordination number: 2.4), showing Nb-Si length at 0.330 nm (coordination number: 1.9). There are two kinds of Nb-Nb bonds at 0.334 nm and 0.368 nm. These values are similar to those of observed in Nb_2O_5-monolayers on SiO_2 and Nb-acid monolayers on SiO_2 [11,14]. The coordination numbers were estimated to be 0.9 and 1.3, respectively (both: *ca.* one). It is likely that two dimeric units were combined together to a tetramer on the lowest-surface are SiO_2. The Nb-O bond at 0.216 nm is similar to 0.213 nm and 0.218 nm for the bridging oxygen in $Nb_2(1)$ and $Nb_2(2)$. The Nb atoms are situated in a pentavalent state as the highest oxidized species. Thus, the catalyst $Nb_2(4)$ is proposed to have a tetrameric structure having mono-μ- and di-μ-oxygen bridges as shown in Figure 7.

The distinct peak due to 1s→4d transition was observed for $Nb_2(1)$, $Nb_2(2)$ and $Nb_2(3)$, but not for $Nb_2(4)$ in the Nb K-edge XANES spectra as shown in Figure 6. The pre-edge peak definitely appears when Nb is located in tetrahedral or distorted tetrahedral symmetry, which implies that Nb=O double bonds are

included in $Nb_2(1)$, $Nb_2(2)$ and $Nb_2(3)$, but may not in $Nb_2(4)$. These results are compatible with the EXAFS results in Table 1 and support the strcutures in Figure 7.

Thus, the structures of Nb sites on SiO_2 were determined by EXAFS and XANES as shown in Figure 7. While the dimeric structure is straightforwardly presented, the tetrameric structure ($Nb_2(4)$) in Figure 7 is tentative. The structure (**4**) was proposed on the basis of the dimer structures and the one-atomic Nb-oxide layers [10,11].

4.2.2. Regulation of intra- and inter-adsorbate dehydration

The Nb dimers $Nb_2(1)$, $Nb_2(2)$, $Nb_2(3)$ and $Nb_2(4)$ all catalyzed the dehydration of ethanol and the selectivities were 91-99 % at 523 K in Table 2. Though the differences in dehydration acitvities were observed in each catalysts, the reason is still unclear. However, the differences in activities for each support were obserbed both attached catalysts and impregnation catalysts with same trend (the highest acitivity was achieved by supported on Aerosil 300, and the lowest activity was achieved by supported on Fuji-Davison micro bead silica gel 4B). Thus, the differences in acitivities of dehydration seemed not due to the differences in active structures around Nb atom but due to the native of support. To compensate these differences in activity, the ratio of the rates were calculated also listed in Table 2. The ratio of the rate of diethyl ether (inter-dehydration) to the rate of ethene (intra-dehydration) changed by moving the structure from $Nb_2(1)$ to $Nb_2(4)$ (1.8, 1.5, 0.93 and 2.9 for $Nb_2(1)$, $Nb_2(2)$, $Nb_2(3)$ and $Nb_2(4)$, respectively), whereas the corresponding conventional impregnation Nb catalysts obtained by the silicas identical to the attached catalysts did not show

any differences in the ratio. Thus the selectivity of dehydration can be controlled by designed, active structures, not by traditional ill-defined catalyst surfaces. It has been demonstrated by EXAFS, XANES and kinetics that ethene and diethyl ether on $Nb_2(1)$ are produced by the scheme in Figure 8 [9]. Adsorption isotherms of ethanol at 523 K on $Nb_2(1)$, $Nb_2(2)$, $Nb_2(3)$ and $Nb_2(4)$ followed the Langmuir type and the amount of saturation was equal to the amount of Nb atom on all four catalysts, suggesting that the adsorption of ethanol did not affect the second molecule of ethanol adsorbing to the dimer unit. Thus the amount of species $[S_1Et_1]$ and $[S_0Et_2]$ are statistically determined by the ethanol pressure, where $[S_1Et_1]$ and $[S_0Et_2]$ represents a ethanol molecule adsorbed on a Nb dimer unit and two ethanol molecules adsorbed on a Nb dimer unit, respectively. The rates of diethyl ether formation and ethene formation are represented by equations (1) and (2),

$$v(\text{diethyl ether}) = k_1[S_0Et_2] \quad (1),$$

$$v(\text{ethene}) = k_2[S_1Et_1] + 2k_3[S_0Et_2] \quad (2),$$

where k_1, k_2 and k_3 are the first-order rate constants. The rate constants were determined by fitting the eqns (1) and (2) to the observed kinetic data, while the ethanol pressure varies from 0.4 to 4.0 kPa to control $[S_1Et_1]$ and $[S_0Et_2]$. The obtained rate constants are shown in Table 2. The ratios k_2/k_3 for $Nb_2(1)$, $Nb_2(2)$, $Nb_2(3)$ and $Nb_2(4)$ were observed to be 2.6-7.1 in Table 2. This indicates that the intra-dehydration of the first ethanol is suppressed when the second ethanol molecule adsorbs on the adjacent Nb atom in a dimer unit. The ratios k_1/k_3 for all the catalysts in Table 2 were larger than unity (2.1-13), showing a

preferable inter-dehydration on the two-ethanols adsorbed sites (S_0Et_2), or suppression for intra-dehydration on the two-ethanols adsorbed sites. These results demonstrate that a character of $Nb(OH)(OC_2H_5)$ monomer (S_1Et_1) is considerably modified or lost by the co-adsorption effect (adsorption on the adjacent Nb atom). The effect strongly depends on the Nb structure.

In the case of the tetrameric structure $Nb_2(4)$, the dehydration mechanism must be a little different from Figure 8 because there is no Nb=O bond. Ethanol may adsorb on the two-oxygen-bridged sites like the esterification on the niobic-acid monolayer catalyst [14], followed by adsorption of second ethanol molecule to the Nb site possessing Nb-OEt bond as shown in Figure 9. This kind of regulation in the rate constants and rates was not achieved with the conventional impregnation Nb catalysts.

4.2.3. Structural change of Nb sites

The structure change of Nb sites during ethanol dehydration on $Nb_2(3)$ was found by in situ EXAFS. The details of the dynamic structure change will be reported in chapter 5, but the preliminary results are described here.

After ethanol admission to $Nb_2(3)$ at 523 K for 5 min, the gas phase was evacuated for 10 s and the catalyst was cooled down to 293 K rapidly. The obtained sample was monitored by EXAFS at 70 K. The EXAFS data were analyzed by the curve fitting method above mentioned. In contrast to no Nb-Nb bonding in the $Nb_2(3)$, the Nb-Nb bond was observed at 0.308 nm by ethanol adsorption at 523 K. Admission of ethanol to $Nb_2(3)$ may lead to the formation of ethoxyl and hydroxyl ligands at each Nb=O site, followed by the dehydration of the two hydroxyl ligands to produce the oxygen-bridged Nb dimer structure. The dimer structure with

ethoxyl groups was converted again to the $Nb_2(3)$ structure without Nb-Nb bond as proved by EXAFS, evolving ET and DE at 523 K. It is suggested that the dehydration of ethanol on $Nb_2(3)$ proceeds in conjunction with a dynamic structure change of Nb site involving formation-breaking of Nb-Nb bond.

4.3. Conclusions

(1) The attached Nb-dimer catalysts were prepared by using a dimeric complex $[Nb(\eta^5\text{-}C_5H_5)H\text{-}\mu\text{-}(\eta^5,\eta^1\text{-}C_5H_4)]_2$ and four kinds of SiO_2.

(2) These Nb catalysts were characterized by EXAFS to have different Nb-Nb bonds and local structures around Nb atom.

(3) Adsorption of ethanol on the Nb dimer catalysts produced the Nb-OH and $Nb\text{-}OC_2H_5$ on each Nb atom. The rate constant of intra-adsorbate dehydration reduced by adsorption of a second ethanol adsorbed on the adjacent Nb atom through adsorbate-adsorbate or Nb-Nb interaction.

(4) The ratio of the rate constants for intra- and inter-adsorbate dehydration (selectivity) is referred to Nb-Nb distance and bond conformation in Nb sites, and also to Nb structure chemically attached to SiO_2 surface.

(5) In the dimeric Nb catalysts, the longer the Nb-Nb distance, the more the rate constant for the inter-dehydration reaction of ethanol reduced compared to that for the intra-dehydration reaction.

References

[1] Yu.I.Yermakov, B.N.Kuznetsov and V.A.Zakharov, Catalysis by Supported Complexes, Elsevier, Amsterdam, 1981.

[2] Y.Iwasawa (ed.), Tailored Metal Catalysts, Reidel, Dortrecht, 1986.

[3] Y.Iwasawa, Adv. Catal., 35(1987)187.

[4] F.R.Hertley, Supported Metal Complexes, Reidel, Dortrecht, 1985.

[5] B.C.Gates, L.Guczi and H.Knözinger (eds.), Metal Clusters in Catalysis, Stud. Surf. Sci. Catal., Vol. 29, Elsevier, Amsterdam, 1986.

[6] M.Nishimura, K.Asakura and Y.Iwasawa, J. Chem. Soc., Chem. Commun., (1986)1660.

[7] M.Nishimura, K.Asakura and Y.Iwasawa, Proc. 9th Inter. Congr. Catal., IV(1988)1842.

[8] N.Ichikuni, K.Asakura and Y.Iwasawa, J. Chem. Soc., Chem. Commun., (1991)112.

[9] N.Ichikuni and Y.Iwasawa, Proc. 10th Inter. Congr. Catal., Vol. A (1993)2427.

[10] M.Shirai, N.Ichikuni, K.Asakura and Y.Iwasawa, Catal. Today, 8(1990)57.

[11] K.Asakura and Y.Iwasawa, J. Phys. Chem., 95(1991)1711.

[12] K.Asakura and Y.Iwasawa, Chem. Lett., (1986)859.

[13] K.Asakura and Y.Iwasawa, Chem. Lett., (1988)633.

[14] M.Shirai, K.Asakura and Y.Iwasawa, J. Phys. Chem., 95(1991)9999.

[15] N.Ichikuni, K.Asakura and Y.Iwasawa, *J. Chem. Soc., Chem. Commun.*, (1991)112.

Table 1. Curve fitting results for the attached Nb dimer catalysts

catalyst	bond	r[a] / nm	N[b]	ΔE_o[c] / eV	DW[d] / nm
	Nb=O	0.179±0.003	0.6±0.3	-5.0	0.008
	Nb-O	0.193±0.002	1.9±0.3	0.0	0.005
Nb_2(1)	Nb-O	0.213±0.003	1.1±0.2	9.0	0.005
	Nb-Nb	0.303±0.002	0.9±0.2	-1.0	0.006
	Nb-Si	0.328±0.002	2.3±0.2	3.0	0.003
	Nb=O	0.180±0.002	0.6±0.3	1.8	0.008
	Nb-O	0.195±0.003	1.6±0.3	-1.0	0.004
Nb_2(2)	Nb-O	0.218±0.003	0.9±0.2	9.0	0.004
	Nb-Nb	0.308±0.002	0.9±0.2	0.0	0.008
	Nb-Si	0.330±0.002	2.3±0.2	6.1	0.003
	Nb=O	0.173±0.003	0.5±0.4	9.0	0.008
Nb_2(3)	Nb-O	0.197±0.002	2.6±0.4	5.0	0.005
	Nb-O	0.228±0.003	0.7±0.2	9.0	0.004
	Nb-Si	0.336±0.003	1.7±0.3	5.9	0.003
	Nb-O	0.190±0.003	2.4±0.3	-8.5	0.008
	Nb-O	0.216±0.003	2.1±0.3	9.0	0.009
Nb_2(4)	Nb-Nb	0.334±0.002	0.9±0.2	-4.9	0.006
	Nb-Nb	0.368±0.002	1.3±0.2	7.7	0.008
	Nb-Si	0.330±0.003	1.9±0.3	8.9	0.004

a: bond distance, b: coordination number, c: difference between model compound and experimental threshold energies, d: Debye Waller factor.

Table 2. Catalytic activities, rate constants and selectivities for ethanol dehydration at 523 K

catalyst	rate[a] DE	rate[a] ET	v(DE)/v(ET)	selec.*/%	rate constant** / 10^{-3}min^{-1} k_1	k_2	k_3	k_1/k_3	k_2/k_3
Nb_2(1)	7.3	4.0	1.8	96.2	8.0	4.7	1.8	4.4	2.6
Nb_2(2)	14	9.3	1.5	98.5	14	11	4.2	3.4	2.6
Nb_2(3)	2.2	2.3	0.93	91.2	3.9	2.5	1.9	2.1	1.3
Nb_2(4)	6.7	2.3	2.9	95.0	8.9	5.0	0.7	13	7.1

a: 10^{-5}mol min^{-1}g-Nb^{-1}; ethanol pressure: 3.3 kPa,

*r(dehydration)/r(dehydration)+r(dehydrogenation);

**first-order rate constant: see Figure 8.

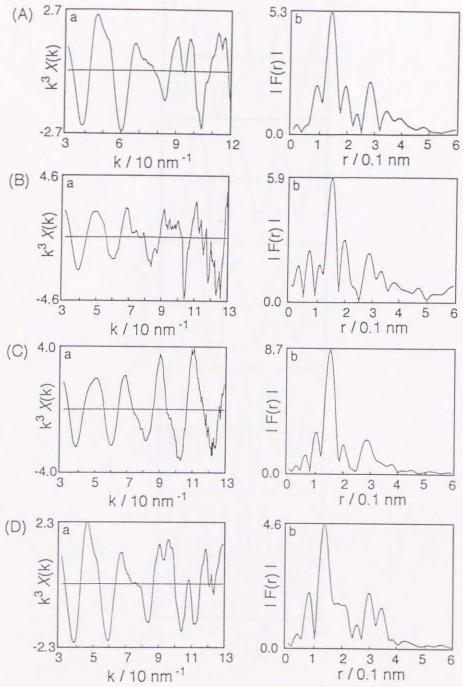

Figure 1. EXAFS spectra of the attached Nb dimer catalysts Nb_2(1) (A), Nb_2(2) (B), Nb_2(3) (C) and Nb_2(4) (D); (a)k^3-weighted oscillations, (b)Fourier transforms.

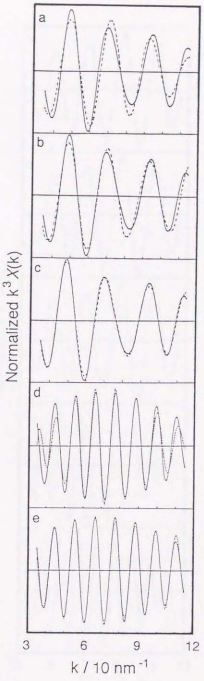

Figure 2. Curve fitting analyses of the EXAFS data for $Nb_2(1)$ (solid line: obs., broken line: calc.); (a)one-wave (Nb-O), (b)two-waves (Nb-O, Nb-O), (c)three-waves (Nb-O, Nb-O, Nb-O), (d)one-wave (Nb-Nb), (e)two-waves (Nb-Nb, Nb-Si).

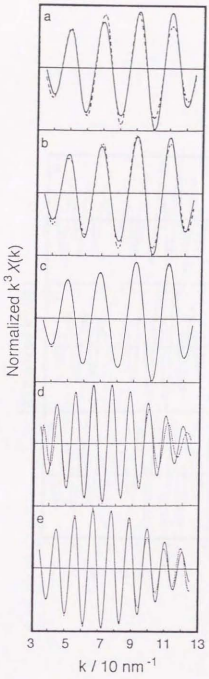

Figure 3. Curve fitting analyses of the EXAFS data for Nb_2(3) (solid line: obs., broken line: calc.); (a)one-wave (Nb-O), (b)two-waves (Nb-O, Nb-O), (c)three-waves (Nb-O, Nb-O, Nb-O), (d)one-wave (Nb-Nb), (e)one-wave (Nb-Si).

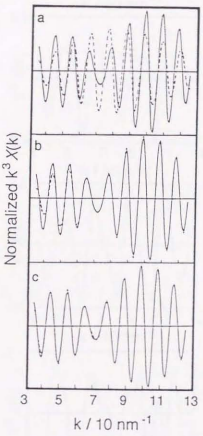

Figure 4. Curve fitting analyses of the EXAFS data for Nb_2(4) (solid line: obs., broken line: calc.); (a)one-wave (Nb-Nb), (b)two-waves (Nb-Nb, Nb-Nb), (c)three-waves (Nb-Nb, Nb-Nb, Nb-Si).

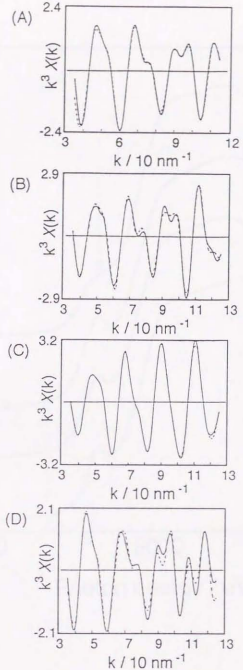

Figure 5. Curve fitting analyses of the EXAFS data for Nb_2(**1**) (A), Nb_2(**2**) (B), Nb_2(**3**) (C) and Nb_2(**4**) (D) (solid line: obs., broken line: calc.).

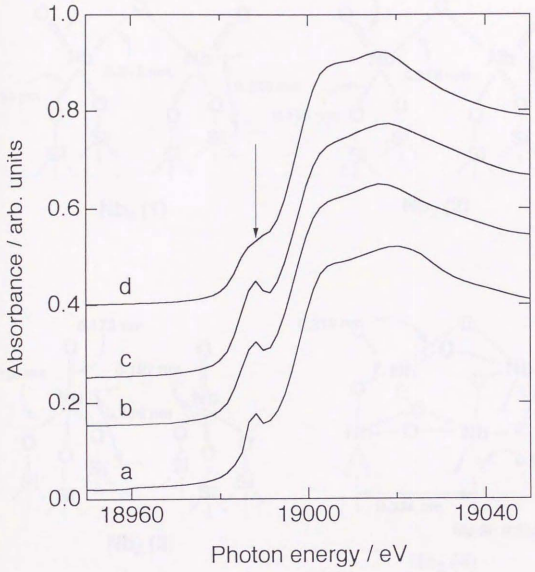

Figure 6. Nb K-edge XANES spectra for the attached Nb dimer catalysts; the arrow represents the 1s→4d transition peak; (a)Nb_2(**1**), (b)Nb_2(**2**), (c)Nb_2(**3**) and (d)Nb_2(**4**).

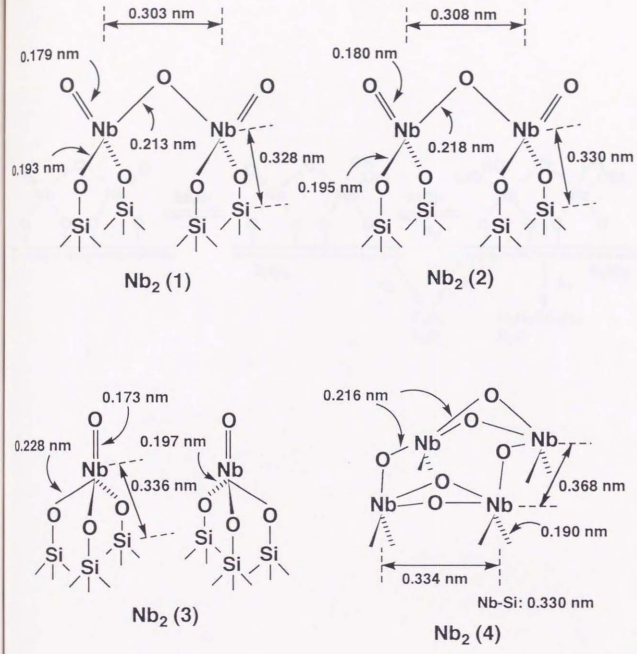

Figure 7. Structures of Nb dimers on SiO_2 (O-Si≡ is not shown for Nb_2(4)).

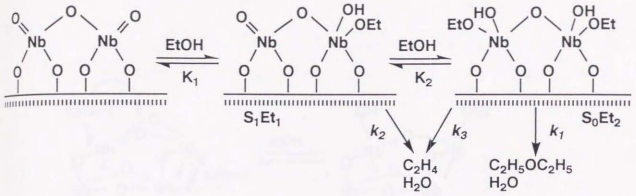

Figure 8. Scheme for ethanol dehydration on Nb dimer catalyst.

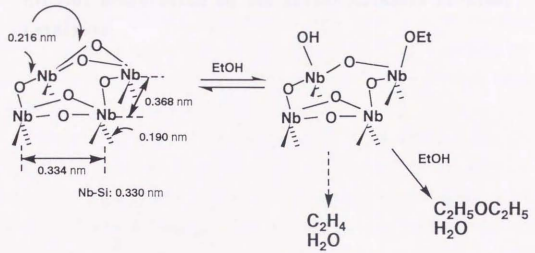

Figure 9. Scheme for ethanol dehydration on Nb_2(4) catalyst (O-SiΞ is not shown).

5. Observation of the Dynamic Change in Active Sites During Ethanol Dehydration on the Silica-Attached Nb-Dimer Catalysts

5.1. Introduction

The attached metal catalysts which are prepared by reactions between suitable organometallic compounds and inorganic oxides, followed by various chemical treatments depending on what kind of active surface structures should be demanded, can provide novel information on the genesis of solid catalysis and a new way of the developments of desired catalysts [1-6]. The use of such catalysts which possess chemically and structurally controlled surface may also bring about the information of elucidating the catalytic mechanism involving dynamic structure change of active sites on an atomic scale [6-8].

Conventional impregnation niobium catalyst and niobium oxide bulk catalyst have been thought as relatively inert and studied largely from the view points of support effects on metal catalysis like a strong metal-support interaction (SMSI) [9-15] or acidic properties at low temperatures below 400 K [16-18]. However, attached Nb monomer catalysts prepared from $Nb(\eta^3\text{-}C_3H_5)_4$ and inorganic oxides like SiO_2 and TiO_2 have been demonstrated to be the first active niobium sample for catalytic ethanol dehydrogenation [8,19].

Recently, Nb oxide and its mixed oxide catalysts have been extensively studied. One-atomic layer niobia on SiO_2 was prepared by the reaction of $Nb(OC_2H_5)_5$ with SiO_2 surface [20-22]. EXAFS revealed that the surface Nb-oxide layers are somewhat distroted by a structural mismatch and a strong Nb-O-Si interaction and the distortion should be released by the creation of the coordinatively unsaturated Nb sites, showing Lewis acidic catalysis for the intra-dehydration of ethanol [20-22]. More recently, the surface Nb-oxide pahse which was prepared by using

Nb-ethoxide or Nb-oxalate as precursors was characterized by means of in situ Raman [23] and FT-IR [24,25], where the highly distorted NbO_6 octahedral structure was present. Datka *et al.* characterized oxide-supported Nb_2O_5 catalysts prepared by use of Nb-oxalate/oxalic acid aqueous solution by FT-IR spectra of chemisorbed pyridine, and concluded that the concentrations of Lewis acid sites and Brönsted acid sites depend on the surface Nb coverage [26]. Burke and Ko prepared a series of composite oxides containing Nb_2O_5 and SiO_2 by using Nb-ethoxide, and examined the relationship between their acidity and the structure around Nb atom. They proposed that the tetrahedral Nb species with Nb=O bond shows a strong Lewis acidity and the highly distorted octahedral species has a moderately strong Lewis acidity [27]. The additive effects of Nb oxides have also been studied in oxidehydrogenations of ethane and propane. Desponds *et al.* reported that the oxidehydrogenation of ethane on Mo-V mixed oxide was considerably enhanced by Nb addition [28]. The oxidative dehydrogenation of propane over the series of oxides, such as lanthane, magnesia, zirconia and titania, Smits *et al.* found that Nb_2O_5 gave the best performance of the series with a selectivity of 76 % to propene and a conversion of propane of 2 % at a temperature of 859 K [29]. Ross *et al.* has appeared that Nb_2O_5 and Nb_2O_5-modified catalysts, when used in high-temperature oxidation process, can exhibit relatively high selectivities compared with more conventional catalysts [30].

The catalytic reaction mechanism has been studied in the most detail on the attached Nb monomer catalyst for ethanol dehydrogenation. Ethanol adsorbes on the Nb=O site to form Nb-OH and $Nb\text{-}OC_2H_5$ groups, but this species was too stable under vacuum and it did not decompose at the reaction temperatures 400-523 K.

The species is decomposed to ethene and water (dehydration) only above 600 K. However, in the presence of a second ethanol adsorbed on the Nb site, the Nb-ethoxide species is readily dehydrogenated to form acetaldehyde and hydrogen, where the switchover of reaction path from dehydration to dehydogenation was induced by the coexistence of the second ethanol molecule [8]. This finding of the new reaction mechanism tempted us to examine the catalytic effect of the second Nb atom instead of the second ethanol molecule in ethanol reaction. We have prepared the Nb dimers on SiO_2 by use of $[Nb(\eta^5\text{-}C_5H_5)H\text{-}\mu\text{-}(\eta^5,\eta^1\text{-}C_5H_4)]_2$ as a precursor. It has been demonstrated that acid/base catalytic properties can be controlled by the nucleation of active sites from one Nb atom to two Nb atoms [31-33]. In the dimer catalysis it is expected that the catalytic properties are changed by Nb-Nb distance of the dimers and local structure around Nb atom, and hence modified by cooperation of two adjacent Nb sites.

In this chapter, I will report (1)four different structures of Nb dimers attached on SiO_2, (2)their catalysis for the intra- and inter-dehydration of ethanol, and (3)the structural change in Nb sites during the catalytic reaction.

5.2. Results and Discussion

5.2.1. Structures and catalytic properties of the catalysts

The structures of Nb sites on SiO_2 were determined by EXAFS and XANES as shown in Figure 1. While the dimeric structure is straightforwardly presented, the tetrameric structure (Nb_2(**4**)) in Figure 1 is tentative. The structure (**4**) was proposed on the basis of the dimer structure and one-atomic Nb-oxide layers

[22,31].

The Nb dimers $Nb_2(1)$, $Nb_2(2)$, $Nb_2(3)$ and $Nb_2(4)$ all catalyzed the dehydration of ethanol and the selectivities were 91-99 % to produce diethyl ether (DE) and ethene (ET) at 523 K in Table 1 [34]. The ratio of the rate of DE (inter-dehydration) to the rate of ET (intra-dehydration) changed by moving the structure from $Nb_2(1)$ to $Nb_2(4)$ (1.8, 1.5, 0.93 and 2.9 for $Nb_2(1)$, $Nb_2(2)$, $Nb_2(3)$ and $Nb_2(4)$, respectively), whereas the corresponding conventional impregnation Nb catalysts obtained by the silicas identical to the attached catalysts did not show any difference in the ratio. Thus the selectivity of dehydration can be controlled by designed, active structures, not by traditional ill-defined catalyst surfaces. The ratio was decreased by separating Nb-Nb distance except for $Nb_2(4)$ possessing not dimeric structure but tetrameric structure. It has been demonstrated by EXAFS, XANES and kinetics that ethene and diethyl ether on $Nb_2(1)$ are produced by the scheme in Figure 2 [33,34]. Adsorption isotherms of ethanol at 523 K on $Nb_2(1)$, $Nb_2(2)$, $Nb_2(3)$ and $Nb_2(4)$ followed the Langmuir type and the amount of saturation was equal to the amount of Nb atom on all four catalysts, suggesting that the adsorption of ethanol did not affect the second molecule of ethanol adsorbing to the dimer unit. Thus it seemed that ethene and diethyl ether formation are depicted as the scheme in Figure 2 with the rate equations (1) and (2).

$$v(\text{diethyl ether}) = k_1[S_oEt_2] \quad (1),$$

$$v(\text{ethene}) = k_2[S_1Et_1] + 2k_3[S_oEt_2] \quad (2),$$

where k_1, k_2 and k_3 are the first-order rate constants, and $[S_0Et_2]$ and $[S_1Et_1]$ are the Nb dimer unit adsorbing two ethanol molecules and one ethanol molecule, respectively. Rate constants were determined by fitting the equations (1) and (2) to the experimental data and listed in Table 1. The ratios k_2/k_3 for Nb_2(1), Nb_2(2), Nb_2(3) and Nb_2(4) were observed to be 2.6-7.1 (larger than 1) in Table 1. This indicates that the intra-dehydration is suppressed when another ethanol molecule adsorbs on the adjacent Nb atom in a dimer unit. The ratios k_1/k_3 for all the catalysts in Table 1 were also larger than unity (2.1-13), showing a preferable inter-dehydration on the two-ethanol adsorbed sites. These results demonstrate that a character of $Nb(OH)(OC_2H_5)$ monomer is considerably modified or lost by the co-adsorption effect (adsorption on the adjacent Nb atoms). The more separating the Nb-Nb distance became, the smaller the ratios of k_2/k_3 and k_1/k_3 became except for the case of Nb_2(4). As limited to the dimeric structure, the regulation of intra- and inter-dehydration was performed by changing the Nb-Nb separation. The effect strongly depends on the Nb structure, especially the Nb-Nb distance.

In the case of the tetrameric structure Nb_2(4), the dehydration mechanism must be a little different from Figure 2 because there is no Nb=O bond and the coordiation around Nb atom is more dense. Ethanol may adsorb on the two-oxygen-bridged sites like the esterification on the niobic-acid monolayer catalyst [35], followed by second ethanol adsorption to Nb-OEt site as shown in Figure 3. Thus, the inter-adsorbate dehydration was preferred on Nb_2(4). This kind of regulation in the rate constants and rates was not achieved with the conventional impregnation Nb catalysts.

5.2.2. Structural change in catalytic reaction

$Nb_2(3)$ possesses no Nb-Nb bonding between the adjacent Nb atoms, which may indicate that the Nb species are distributed in a monomeric form. At least there is no evidence on Nb-Nb interaction at SiO_2 surface. However, this may be strange from the catalytic viewpoint. Because, the Nb monomers on SiO_2 have been demonstrated to be active and selective for the dehydrogenation of ethanol, not for the dehydration [8,19]. This is also true for the Nb monomers on TiO_2 [8,19], and the local structure around Nb atom on TiO_2 is similar to the $Nb_2(3)$ structure as shown in Figure 4. Therefore, it seems that the $Nb_2(3)$ catalyst should produce acetaldehyde (dehydrogenation product) as a main product in ethanol reaction by the self-assisted dehydrogenation mechanism [8]. Although the static structure of $Nb_2(3)$ resembles Nb monomer/TiO_2, the catalysis of $Nb_2(3)$ is entirely different from that of Nb monomer/TiO_2. To clarify this problem in relation to the genesis of catalysis, we examined the structural change of Nb sites in the course of catalytic ethanol dehydration by means of EXAFS.

A large amount of H_2O was formed at the initial stage of reaction. The amount of produced water at 3 min at 523 K and $P(C_2H_5OH)$= 3.3 kPa was approximately equal to the Nb dimer unit as shown in Figure 5. After the rapid formation of water, the water was steadily produced, which amount corresponded to the amount of the dehydration products. After the initial evolution of water, the catalyst was quenched by cooling it to room temperature, accompanied with evacuation of gas phase. The EXAFS spectrum for the sample thus obtained is shown in Figure 6(A). The EXAFS data were analyzed by the curve fitting method as above

mentioned. The best fitting curve is shown in Figure 6 and the bond distances and the coordination numbers are listed in Table 2. The Nb=O double bond disappeared and a Nb-Nb bond of 0.308 nm with the coordination number of 1.0 newly appeared. The reduction of the 1s→4d transition peak height in the XANES spectrum upon ethanol adsorption was observed, supporting the vanishment of Nb=O bond observed by EXAFS. Ethanol adsorbed on the Nb=O sites producing Nb-OH and Nb-OC_2H_5 [8,33,34]. When Nb-OH species thus formed are located closely each other, the dehydration from two adjacent Nb-OH species can readily take place at 523 K. As a result, Nb-O-Nb bonds are formed to make a dimeric structure as shown in Figure 7. The Nb-bridging O bond was observed at 0.220 nm and the Nb-Nb length was 0.308 nm, both being similar to those for Nb_2(2). The coordination number for Nb-O of 0.198 nm was determined to be 3.2 which is larger by 0.6 than 2.6 for the original catalyst (3). It suggests that an additional Nb-O bond at 0.198 nm (Nb-OC_2H_5) was formed upon ethanol adsorption, which agrees with the results of IR and XANES. Accordingly, the structural change by ethanol adsorption at 523 K accompanied with H_2O evolution is illustrated in Figure 7.

When the fully ethanol-adsorbed Nb dimers were decomposed, ethene and diethyl ether were evolved at 523 K. After the formation of ethene and diethyl ether was completed, the EXAFS spectrum of the sample was measured. The EXAFS oscillation, its Fourier transform and curve fitting analysis are shown in figure 6(B). The best-fit result is listed in Table 2. The Nb=O bond was regenerated and the Nb-Nb bond disappeared. It is evident from Table 2 and Figure 1 that the original structure of Nb_2(3) was reproduced.

The adsorption of ethanol on $Nb_2(3)$ followed the Langmuir type, exhibiting that there is nearly no effect on adsorbing the second ethanol molecule to the Nb dimer unit on which one ethanol was adsorbed. Thus the amount of species $[S_1Et_1]$ and $[S_0Et_2]$ was determined by using the adsorption isotherm of ethanol at 523 K. For example, the pressure of ethanol was situated as 3.7 kPa, $[S_0Et_2]$ and $[S_1Et_1]$ became almost 1 and 0, respectively. Since the rate of diethyl ether formation and ethene formation was expressed as eqns (1) and (2), respectively, the rate constants were statistically determined from the rates of various ethanol pressures. These values are collected under ethanol circumstances namely in catalytic conditions are listed in Table 3(b). To examine whether these rate constants correspond to those of each elementary steps, the rate constants were determined under another conditions as follows: The pressure of ethanol was changed as 0.3 kPa or 4.0 kPa at 523 K to regulate the amount of $[S_1Et_1]$ and $[S_0Et_2]$. After the catalyst was exposed to the ethanol for a while, the gas phase was evacuated and the production of ethene and diethyl ether was monitored. Under this condition, the dehydration of ethanol was surely proceeded but not catalytically. Thus the rate constants determined under this condition was listed in Table 3(a). Both values listed in Table 3(a) and (b) are in fair agreement. Thus the reaction scheme for ethanol dehydration on $Nb_2(3)$ is proposed as Figure 7. At first, the catalyst shows no Nb-Nb coordination determined by EXAFS. Ethanol is adsorbed on Nb=O double bond site to produce Nb-OH and $Nb-OC_2H_5$. As both Nb=O site in the dimer unit is filled with adsorbed ethanol, dehydration is occurred from Nb-OH on both Nb=O site to form Nb-O-Nb dimeric feature. When ethoxyl ligand is consumed by the dehydration reaction, the monomeric

structure is reproduced. It is suggested that the dehydration of ethanol on $Nb_2(3)$ proceeds in conjunction with a dynamic structural change in Nb site involving formation-breaking of Nb-Nb bond. Although the length between Nb and support oxygens were almost unchanged, Nb-Si bond length was also changed largely as 0.336 nm and 0.326 nm for monomeric structure and dimeric structure, respectively, as illustrated in Figure 7. It is supposed that the strcutural change in the monomer and dimer site on the dehydration of ethanol caused the movement of the support surface.

5.3. Conclusions

(1) The attached Nb-dimer catalysts supported on four kinds of silica were prepared by using a dimeric complex $[Nb(\eta^5\text{-}C_5H_5)H\text{-}\mu\text{-}(\eta^5,\eta^1\text{-}C_5H_4)]_2$. These Nb catalysts were characterized by EXAFS to have different Nb-Nb bonds and local structures of active site around Nb atom.

(2) In the dimeric Nb catalysts, the longer the Nb-Nb distance became, the more diminished the inter-dehydration reaction of ethanol compared to the intra-dehydration activity accompanied with the change in rate constants.

(3) Although $Nb_2(3)$ had no Nb-Nb bond (monomer pairs) under the static conditions, the Nb-Nb bond at 0.308 nm appeared under the catalytic reaction conditions and disappeared when the adsorbed ethanol was consumed by the reaction.

(4) The catalytic ethanol dehydration on $Nb_2(3)$ proceeds in conjunction with a dynamic structural change of formation-break cycle of Nb-Nb bonds.

(5) A local structure rearrangement at the Nb-O-Si interface on

SiO_2 is suggested to occur in the course of the catalytic reaction.

References

[1] Yu.I.Yermakov, B.N.Kuznetsov and V.A.Zakharov, *Catalysis by Supported Complexes*, Elsevier, Amsterdam, 1981.

[2] Y.Iwasawa (ed.), *Tailored Metal Catalysts*, Reidel, Dordrecht, 1986.

[3] Y.Iwasawa, *Adv. Catal.*, **35**(1987)187.

[4] B.C.Gates, L.Guczi and H.Knözinger (eds.), *Metal Clusters in Catalysis, Stud. Surf. Sci. Catal.*, Vol. 29, Elsevier, Amsterdam, 1986.

[5] F.R.Hertly, *Supported Metal Complexes*, Reidel, Dordrecht, 1985.

[6] Y.Iwasawa, *Catal. Today*, **18**(1993)21.

[7] Y.Iwasawa, K.Asakura, H.Ishii and H.Kuroda, *Z. Phys. Chem.*, **144**(1985)105.

[8] M.Nishimura, K.Asakura and Y.Iwasawa, *Proc. 9th Inter. Congr. Catal.*, **IV**(1988)1842.

[9] S.J.Tauster and S.C. Fung, *J. Catal.*, **55**(1978)29.

[10] E.I.Ko, M.Hupp and N.J.Wagner, *J. Catal.*, **86**(1984)315.

[11] K.Kunimori, Y.Doi, K.Ito and T.Uchijima, *J. Chem. Soc., Chem. Commun.*, (1986)965.

[12] R.T.K.Baker, S.J.Tauster and J.A.Dumesic (eds.), *Strong Metal-Support Interactions, ACS Symp. Ser.* No. 298, 1986.

[13] H.Yoshitake, K.Asakura and Y.Iwasawa, *J. Chem. Soc., Faraday Trans. 1*, **84**(1988)4337.

[14] H.Yoshitake, K.Asakura and Y.Iwasawa, *J. Chem. Soc., Faraday Trans. 1*, **85**(1989)2021.

[15] H.Yoshitake and Y.Iwasawa, *J. Catal.*, **125**(1990)227.

[16] T.Iizuka, K.Ogasawara and K.Tanabe, *Bull. Chem. Soc. Jpn.*, **56**(1983)2927.

[17] Z.Chen, T.Iizuka and K.Tanabe, *Chem. Lett.*, (1984)1085.

[18] T.Iizuka, S.Fujie, T.Ushikubo, Z.Chen and K.Tanabe, *Appl. Catal.*, **28**(1986)1.

[19] M.Nishimura, K.Asakura and Y.Iwasawa, *J. Chem. Soc., Chem. Commun.*, (1986)1660.

[20] K.Asakura and Y.Iwasawa, *Chem. Lett.*, (1986)859.

[21] K.Asakura and Y.Iwasawa, *Chem. Lett.*, (1988)633.

[22] K.Asakura and Y.Iwasawa, *J. Phys. Chem.*, **95**(1991)1711.

[23] J.M.Jehng and I.E.Wachs, *J. Phys. Chem.*, **95**(1991)7373.

[24] A.M.Turek, I.E.Wachs and E.DeCanio, *J. Phys. Chem.*, **96**(1992)5000.

[25] M.A.Vuurman and I.E.Wachs, *J. Phys. Chem.*, **96**(1992)5008.

[26] J.Datka, A.M.Turek, J.M.Jehng and I.E.Wachs, *J. Catal.*, **135**(1992)186.

[27] P.A.Burke and E.I.Ko, *J. Catal.*, **129**(1991)38.

[28] O.Desponds, R.L.Keiski and R.A.Somorjai, *Catal. Lett.*, **19**(1993)17.

[29] R.H.H.Smits, K.Seshan and J.R.H.Ross, *ACS Petrol. Chem. Div. Prepr.*, **37**(1992)1121.

[30] J.R.H.Ross, R.H.H.Smits and K.Seshan, *Catal. Today*, **16**(1993)503.

[31] M.Shirai, N.Ichikuni, K.Asakura and Y.Iwasawa, *Catal. Today*, **8**(1990)57.

[32] N.Ichikuni, K.Asakura and Y.Iwasawa, *J. Chem. Soc., Chem. Commun.*, (1991)112.

[33] N.Ichikuni and Y.Iwasawa, *Proc. 10th Inter. Congr. Catal.*, **A**(1993)477.

[34] N.Ichikuni and Y.Iwasawa, *Catal. Today*, **16**(1993)427.

[35] M.Shirai, K.Asakura and Y.Iwasawa, *J. Phys. Chem.*, **95**(1991)9999.

Table 1. Rate constants and selectivities for ethanol dehydration at 523 K

catalyst	selec.*/ %	rate constant** / $10^{-3}min^{-1}$			k_1/k_3	k_2/k_3
		k_1	k_2	k_3		
$Nb_2(1)$	96.2	8.0	4.7	1.8	4.4	2.6
$Nb_2(2)$	98.5	14	11	4.2	3.4	2.6
$Nb_2(3)$	91.2	3.9	2.5	1.9	2.1	1.3
$Nb_2(4)$	95.0	8.9	5.0	0.7	13	7.1

*r(dehydration)/r(dehydration)+r(dehydrogenation); ethanol pressure: 3.3 kPa.

**first-order rate constant: see Figure 2.

Table 2. Curve fitting results for $Nb_2(3)$ after ethanol admission at 523 K (1) and at the end of the reaction (2)

condition	bond	r[a] / nm	N[b]	ΔE_o[c] / eV	DW[d] / nm
	Nb-O	0.198±0.002	3.2±0.3	9.0	0.006
(1)	Nb-O	0.220±0.003	1.4±0.3	9.0	0.005
	Nb-Nb	0.308±0.002	1.0±0.2	8.0	0.005
	Nb-Si	0.326±0.003	2.0±0.3	1.7	0.003
	Nb=O	0.176±0.003	0.5±0.4	9.0	0.008
(2)	Nb-O	0.195±0.002	2.6±0.4	2.0	0.005
	Nb-O	0.230±0.003	0.7±0.2	9.0	0.004
	Nb-Si	0.339±0.003	2.0±0.3	8.0	0.003

a: bond distance, b: coordination number, c: difference between model compound and experimental threshold energies, d: Debye Waller factor; filtering range: 0.10-0.35 nm.

Table 3. Rate constants for ethanol dehydration on $Nb_2(3)$ at 523 K

	rate constant / $10^{-3}min^{-1}$		
	k_1	k_2	k_3
(a)	3.7	2.8	2.1
(b)	3.9	2.5	1.9

(a)determined from each elementary steps, (b)determined from steady state reaction condition, see text.

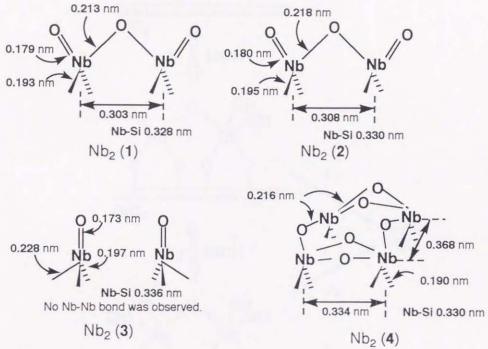

Figure 1. Structures of Nb dimers on SiO_2 (O-Si≡ is not shown for all catalysts).

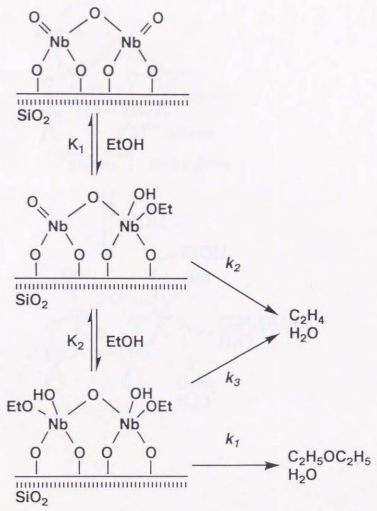

Figure 2. Scheme for ethanol dehydration on Nb dimer catalyst.

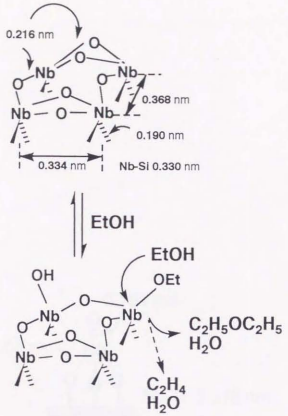

Figure 3. Scheme for ethanol dehydration on Nb_2(4).

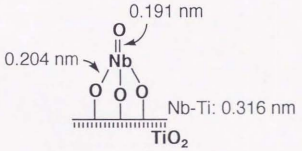

Figure 4. Structure of the TiO_2 attached Nb monomer catalyst.

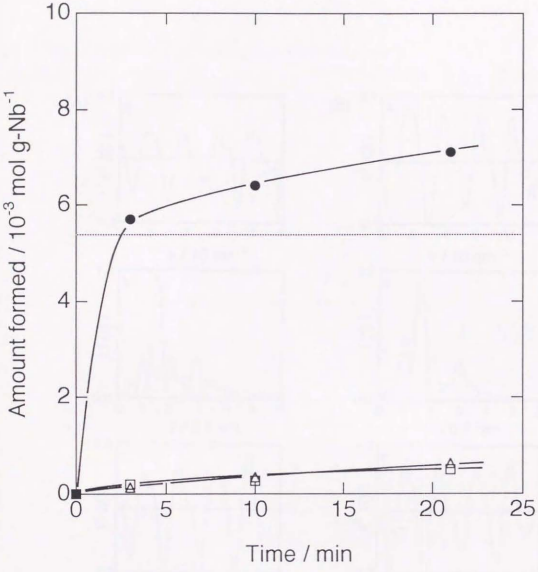

Figure 5. The reaction profile of ethanol dehydration on Nb_2(3); dotted line represents the amount of Nb dimer; (●)water, (△)ethene, (□)diethyl ether.

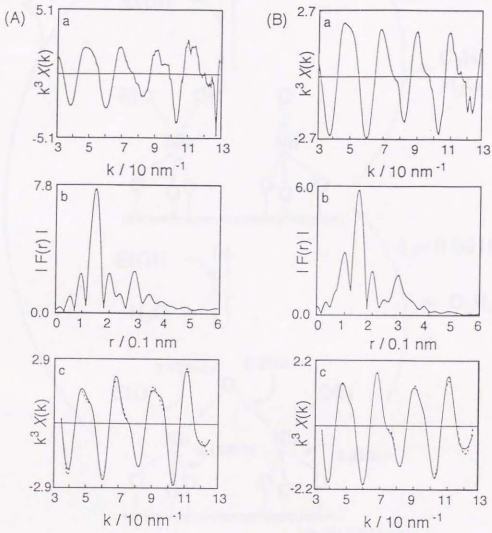

Figure 6. EXAFS spectra of Nb_2(3) after ethanol admission (A) and at the end of the reaction (B); (a)k^3-weighted oscillations, (b)Fourier transforms and (c)curve fitting (solid line: obs., broken line: calc.).

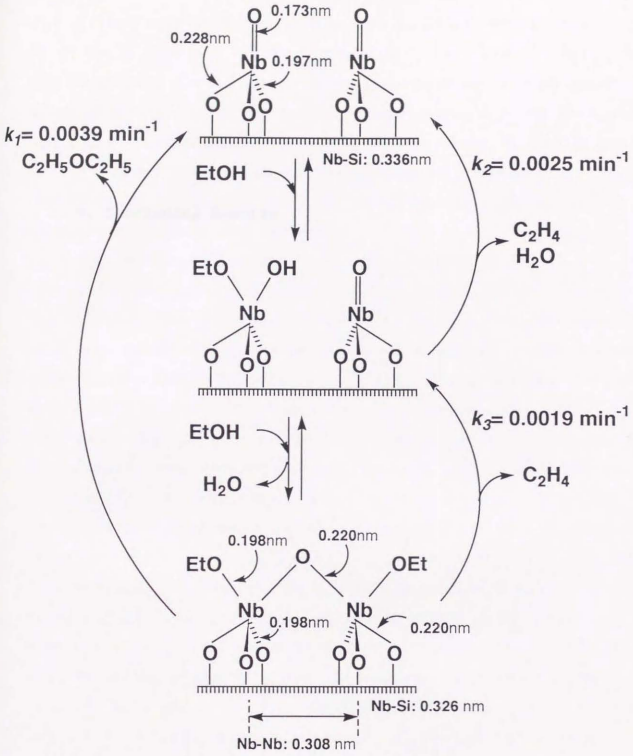

Figure 7. The reaction scheme for ethanol dehydration on Nb_2(3).

6. Concluding Remarks

I have studied on the design and catalysis of the attached Nb dimer catalysts. In chapter 3, I mentioned how different the structures and catalysis are between Nb monomer catalysts and Nb dimer catalysts. The regulation of the rate constants for intra- and inter-dehydration of ethanol by changing the Nb-Nb distances and arrangements was discussed in chapter 4. In chapter 5, the observation of the structural change around Nb site during ethanol dehydration was depicted.

The Nb monomer catalyst has been found to be the first active Nb sample for the catalytic dehydrogenation of ethanol by the self-assisted dehydrogenation mechanism. It was wondered what kind of effect of the second Nb atom instead of the second ethanol molecule on Nb catalysis in ethanol reaction may have existed. I prepared the new silica-attached Nb dimer catalysts for the purpose of finding the effect of the second Nb atom and for understanding the cooperative catalysis of two adjacent Nb atoms as a model for general metal oxide catalysts. Although the local structures of NbO_4 species in the Nb dimer were close to those of the Nb monomers, the catalysis was drastically changed. The regulation of the catalysis from dehydrogenation to dehydration, or equivalently from basic property to acidic property on Nb sites, was achieved by the nucleation of one Nb atom to two Nb atoms in active structures. This was due to (1)electronic effect as Nb in the dimer is more Lewis acidic than Nb in the monomer, and (2)geometric effect as the existence of the second NbO_4 unit and the bridged oxygen in the Nb dimers inhibits the self-assisted dehydrogenation reaction mechanism. The inverse isotope effect for ethene formation through the late-transition state of reaction and the reduction of the rate constant for ethene formation by the second ethanol adsorption on

the adjacent Nb site were also observed.

The regulation of the rate constants for intra- and inter-dehydration of ethanol was thought to be achieved by changing the Nb-Nb distance. For this sake, I prepared Nb dimers on four kinds of silicas to change the structures around Nb atom especially Nb-Nb distances. These Nb catalysts were characterized by EXAFS to have different Nb-Nb bonds and local structures of active Nb sites. The rate constant of intra-adsorbate dehydration reduced by adsorption of a second ethanol on the adjacent Nb atom through adsorbate-adsorbate or Nb-Nb interaction. The ratio of the rate constants for intra- and inter-adsorbate dehydration (selectivity) was referred to Nb-Nb distance and bond conformation in Nb sites, and also to Nb structure chemically attached to silica surface.

Although Nb_2(3) had no Nb-Nb bond (monomer pairs) under the static conditions, the Nb-Nb bond at 0.308 nm appeared under the catalytic reaction conditions and disappeared when the adsorbed ethanol was consumed by the reaction. It was found that the catalytic ethanol dehydration on Nb_2(3) proceeded in conjunction with a dynamic structural change of formation-break cycle of Nb-Nb bonds. A local structure rearrangement at the Nb-O-Si interface on silica was suggested to occur in the course of the catalytic reaction.

I investigated the relationship between structure and catalysis on the designed Nb catalysts in detail. I found the basicity/acidity change in catalysis by the nucleation from one to two Nb atoms in active sites, and the regulation of the rate constant by changing the Nb-Nb distances and arrangements. I observed the formation-break cycle of Nb-Nb bonds in the course of ethanol dehydration. These phenomena could not be observed on

conventional impregnation catalysts but observable on atomically designed catalysts. Atomically designed catalysts may help the understanding of the genesis of solid catalysis and provide regulated catalysis.

参考論文

In-situ d-Electron Density of Pt Particles on Supports by XANES

1. Introduciton

The electronic properties of metal particles are one of the most important ingredients to understand the genesis and mechanism of noble-metal catalysis. The change in the d electron density of metal particles should be essential for metal catalysis since the adsorption or activation of reactants and hence the resultant surface reaction processes are affected largely by the interaction of d electrons with frontier orbitals of reactants. It is often said that static characterization of catalysts produces different results from *in situ* characterization [1-4]. Then, it is important to characterize the d electron density of state under *in situ* conditions. The X-ray absorption near-edge structure (XANES) spectroscopy can provide this information. The white lines of Pt L_{III} and L_{II} edges, stemming from photo-excitation from $2P_{3/2}$ or $2P_{1/2}$ state to 5d state, respectively, have been demonstrated to reflect the unoccupied electron density of the 5d orbital of Pt [4].

We have already investigated the correlation between the activity of Na_2O-doped Pt/SiO_2 catalysts for ethene hydrogenation and the d electron density of the Pt particles under vacuum and ethene [1,2]. The d electron density of Pt under vacuum increased by the addition of Na_2O, indicating electron donation from Na_2O to Pt, whereas it was found that under the reaction conditions (the Pt surface is nearly saturated with ethene at low temperature) most of the d electrons donated from Na_2O moved to adsorbed ethene and as a result, hydrogen (its dissociative adsorption is rate-determining for ethene hydrogenation) feels no change of d electron density of Pt irrespective of the donation of electrons from Na_2O. This may lead to structure insensitive

reaction for ethene hydrogenation on Pt/SiO_2 in an electronic sense.

The d electron density of Pt particles may also be controlled by Pt particle size. This is related with the classification of structure sensitive/insensitive reaction on Pt catalysts. Hydrogenation reaction has been classified to be structure insensitive, but recently opposite results were presented [5].

In this paper, the d electron density of Pt particles in Pt/SiO_2 catalysts under vacuum and under *in situ* conditions, its change by the particle size, and observation of a Pt-H induced peak, are reported by means of *in situ* XANES.

2. Experimental Section

SiO_2(Aerosil 200; surface area: 200 m^2g^{-1} and Aerosil 300: 300 m^2g^{-1}) were used as support. Platinum loading were regulated to 1.5 wt%. Two methods of preparation were applied to change the particle size; one is ion-exchange method using an aqueous solution of $Pt(NH_3)_4Cl_2$, and the other is an impregnation method using an aqueous solution of H_2PtCl_6. Each catalyst was placed in a U-shaped Pyrex glass tube combined with a closed circulating system and treated with oxygen at 573 K for ion exchanged catalysts and at 673 K for an impregnated catalysts, followed by reduction with hydrogen at the same temperature as oxidation. The temperature and duration of the pretreatments were varied to change the size of Pt particles. The particle size was estimated by irreversible hydrogen chemisorption assuming a stoichiometric ratio of H/Pt = 1.

XANES measurements of the catalysts at Pt L_{III} and L_{II} edges

were performed at BL-10B in the Photon Factory at the National Laboratory for High Energy Physics (KEK-PF) (Proposal No. 91-171). The storage ring was operated at 2.5 GeV with the ring current 200-300 mA. Samples were prepared in the closed circulating system and transferred to glass cells with Kapton windows without contacting air. The XANES spectra were measured at room temperature under vacuum, hydrogen of 8.0 kPa, and ethene of 8.0 kPa, in a transmission mode. The synchrotron radiation as monochromatized by Si(311) channel cut monochrometer. The energy calibration was carried out using Pt foil based on Pt inflection points of the L_{III} and L_{II} edges. The data collection was carried out by using the ionization chambers filled with nitrogen for I_o (before sample) and I (after sample), with the length 17 and 34 cm, respectively. Edge jumps of the samples were regulated to about 0.5 for the L_{III} edge.

XANES data were analyzed as follows. Background subtraction from XANES data was performed with the Victoreen's equation

$$\mu t = a_o + a_3\lambda^3 + a_4\lambda^4 \qquad (1),$$

where μt is the absorption coefficient and λ is the wave length. The total amount of unoccupied electron density of d orbital of Pt samples, h_T, was calculated in the following equation [4],

$$h_T = (1 + f_d) h_r \qquad (2),$$

where h_r is unoccupied d electron density of standard Pt (Pt foil) reported to be 0.30-0.40 [6,7]. Thus, f_d can be used as the indicator of unoccupied d electron density of Pt sample. The f_d was expressed as follows,

$$f_d = (\Delta A_{III} + 1.11\Delta A_{II}) / (A_{IIIr} + 1.11A_{IIr}) \qquad (3)$$

$$\Delta A_{III} = A_{III} - A_{IIIr}, \quad \Delta A_{II} = A_{II} - A_{IIr} \qquad (4).$$

Here, A_{III} and A_{II} are the intensities of the white lines at L_{III} and L_{II} edges. A_{IIIr} and A_{IIr} are the corresponding white line

intensities for the reference sample. The intensity of a white line was determined from the result of the fitting with arctangent and Lorentzian functions for the normalized spectrum [8]. The area of the Lorentzian is attributed to the intensity of the white line.

3. Results and discussion

Particle size of supported platinum was varied in the range of 1.0-5.0 nm, which was determined by hydrogen chemisorption at 273 K. The range of particle sizes was wide enough to examine the particle size effect on chemical and physical properties.

The f_d of the supported Pt particles under vacuum is shown in Figure 1. Under vacuum, d electron density of Pt particles was almost constant in the particle size larger than 1.5 nm, where the f_d was 0.07. However, the smaller the particle size in the region below 1.5 nm, the more the Pt particle became electron deficient. The f_d value changed from 0.07 for 1.5 nm to 0.12 for 1.0 nm. Although the shape and intensity of the Pt white line may be influenced by d-s rehybridization, the f_d should reflect the change in d electron density of state arising from particle size, adsorption and metal-support interaction [1-4,9-13]. To reduce the composite effect, we used the same support for 5 catalysts. Although a sample possessing the smallest particle (1.0 nm) was prepared by using a different support (Aerosil 300) from others (Aerosil 200), the difference of the nature of support were not so serious. XPS binding energy (B.E.) of Pt particles also increases below 2 nm [14-17]. These results suggest that the smaller Pt particles (1-2 nm in diameters) are electronically deficient as compared with bulk Pt.

Figure 1 also shows the f_d of the supported Pt particles under reaction-gas atmosphere (ethene or hydrogen). It was observed that the f_d was changed by electron transfer of Pt particle from/to adsorbates. Exposure of the Pt samples to ethene at 293 K caused an upshift of f_d, indicating the withdrawal of d electrons by ethene. On the other hand, the adsorption of hydrogen shifted the d electron states to more rich electron density, suggesting that hydrogen behaved as an electron donor. Comparing these f_d values with those under vacuum, we can obtain the difference of f_d under vacuum and reaction conditions, Δf_d, for each particle size as shown in Figure 2. Since the difference was caused by adsorbates, Δf_d was divided by the amount of chemisorbed ethene or hydrogen on Pt. The normalized $\Delta f_d(\Delta f_d')$ is also shown in Figure 2. The tendency of the particle size effect is similar with both adsorptions, though the direction of electron transfer is opposite. The larger the particle size in the range $\leq$ 3.0 nm, the more the electron transfer between Pt particles and adsorbates increased. These phenomena can be explained partly by the increase of B.E. under vacuum for smaller particles of Pt below 2.0 nm [14-17]. This may weaken the electronic interaction between smaller particles and ethene on the smaller Pt particles than 2.0 nm.

Figure 3 shows the normalized XANES spectra at L_{III} and L_{II} edges under vacuum and 8.0 kPa of H_2. In Figure 3, the fitting analyses by arctangent and Lorentzian for the XANES spectra arealso shown. White lines for the larger particles ($\geq$ 2.0 nm) under both vacuum and hydrogen are characterized by a Lorentzian peak as shown in Figure 3(1). White lines for the particles below 1.5 nm were broadened by H_2 adsorption, so the 2nd Lorentzian function was needed to fit the peak well as shown in

Figure 3(2) and (3). They were reproduced only by two Lorentzian peaks and never by one Lorentzian peak. The 2nd peak was observed in both L_{III} and L_{II} edge spectra. And the new peak position was independent of particle size to be *ca.* 6 eV higher from the inflection point of the edge. The new peak disappeared by evacuation of adsorbed hydrogen and appeared again by H_2 adsorption (Figure 3). Although the thickness effect may distort the white line area as reported by Meitzner *et al.* [18], its effect is estimated to be below *ca.* 5% of the edge jump intensity, but our 2nd peak was much larger than it (*ca.* 10times) as shown in Figure 3(2) and (3). The thickness effect may also lead to a little high values for f_d, which would, however, not change the present discussion based on the relative f_d values and their difference.

The relative areas of 2nd peak normalized by the 2nd peak for the smallest particles with 1.0 nm size at L_{III} edge, are plotted against Pt particle size in Figure 4. The areas of 2nd peak divided by the amount of adsorbed hydrogen were calculated as shown by the solid lines in Figure 4. The peak areas for three samples with the particle size $\leq$ 1.5 nm are on the lines. These results suggest that the new peak is due to the direct interaction between Pt surface and adsorbed hydrogen atoms. Samant and Boudart [19] observed a similar peak at about 9 eV above the edge in the difference XANES spectra between the spectra in H_2 and that in He for Pt/Y zeolite. They claimed that adsorbed hydrogen on the Pt particles created the occupied bonding state below the d band and unoccupied antibonding state above d band. We tentative assign this new peak at *ca.* 6 eV above the edge inflection point to be one due to Pt-H bond by the present arctangent-Lorentzian analysis, though a multiple

exciting mode like shake up can not be excluded. This is supported by the following facts; First, the peak appears only under hydrogen atmosphere and second, the peak areas were linearly correlated with the amount of adsorbed hydrogen.

The 2nd peak due to Pt-H bonding was observable with the particles below 1.5 nm. According to the f_d under vacuum in figure 1, the nature of the Pt particles changed at 1.5-2.0 nm. The amount of d electrons transferred was less with the particle sizes $\leq$ 1.5 nm than for the larger particles. This trend seems reverse to the expected one from the change of f_d and B.E. The reason is not clear at present, but Pt-H bond character may be different with different particle sizes; the hydrogen on Pt particles $\leq$ 1.5 nm may covalently bond with the surface Pt atoms, where electrons do not move to Pt atom so much in net, while hydrogen atoms on Pt particles $\geq$ 2.0 nm can move at the surface, where each H atom may interact multiplly with Pt atoms like at three-fold hollow sites for (111) surface and at four-fold hollow sites for (100) surface.

The different behavior of the Pt particles below and above 1.5 nm in the XANES spectra under H_2 and C_2H_4 was reflected in the kinetic data for ethene hydrogenation. The equilibrium constant for ethene adsorption was smaller with the particles $\leq$ 1.5 nm than for the particles $\geq$ 2.0 nm, which coincides with the results in Figure 2. The activation energy for ethene hydrogenation on the smaller Pt particles $\leq$ 1.5 nm was found to be 16 kJ mol^{-1}, while the activation energy for the larger particles of 2.8 and 5.0 nm was 34 kJ mol^{-1}.

Ethene hydrogenation is a reaction investigated for a long time, but the precise mechanism involving electronic and geometric behaviors of adsorbates by metal-adsorbate and

adsorbate-adsorbate interaction is still the subject of controversy. However, it is to be noted that the d electron density of Pt particles on SiO_2 changed drastically by the coexistence of reactant gas and also by the particle size, which are characterized by *in situ* XANES. Further investigation is needed for comprehensive understanding of the present XANES data.

4. Conclusions

(1)The dependency of d electron density of Pt in Pt/SiO_2 catalysts on the particle size was investigated by means of *in situ* X-ray absorption near-edge structure (*in situ* XANES) spectroscopy. The d electron density of Pt particles was measured under vacuum, H_2 and ethene, to gain information about ethene hydrogenation on Pt/SiO_2.

(2)The intensities of the white lines at L_{III} and L_{II} edges in XANES spectra, which are regarded to reflect the unoccupied density of state, varied with the change of particle size under both vacuum and reaction gas atmospheres. The interaction between Pt particle and adsorbates was weak with small particles below 1.5 nm.

(3)A new peak induced by Pt-H bonding in the XANES spectra under H_2 was observed for the samples with Pt particle size $\lesssim$ 1.5 nm. This is related to the change of the turnover frequency and activation energy for ethene hydrogenation by Pt particle size.

References

[1] H.Yoshitake and Y.Iwasawa, *J. Phys. Chem.*, **95**(1991)7368.

[2] H.Yoshitake and Y.Iwasawa, *J. Catal.*, **131**(1991)276.

[3] H.Yoshitake and Y.Iwasawa, *J. Phys. Chem.*, **96**(1992)1329.

[4] A.N.Mansour, J.W.Cook, Jr. and D.E.Sayers, *J. Phys. Chem.*, **88**(1984)2330.

[5] C.Michel and C.O.Bennett, *Adv. Catal.*, **36**(1989)55.

[6] M.Brown, R.E.Peierls and E.A.Stern, *Phys. Rev. B*, **15**(1977)738.

[7] L.S.Mattheiss and R.Deitz, *Phys. Rev. B*, **22**(1980)1663.

[8] J.A.Horsley, *J. Chem. Phys.*, **76**(1982)1451.

[9] D.R.Short, A.N.Mansour, J.W.Cook, Jr., D.E.Sayers and J.R.Katzer, *J. Catal.*, **82**(1983)299.

[10] P.Gallezot, R.Weber, R.A.Dalla Betta and M.Boudart, *Z. Naturforsch.*, **A34**(1979)40.

[11] T.Fukushima, J.R.Katzer, D.E.Sayers and J.W.Cook, Jr., *Proc. 7th Inter. Congr. Catal.*, (1980)79.

[12] F.W.Lytle, P.S.P.Wei, R.B.Greegor, G.H.Via and J.H.Sinfelt, *J. Chem. Phys.*, **70**(1979)4849.

[13] F.W.Lytle, R.B.Greegor, E.C.Marques, D.R.Sandstrom, G.H.Via and J.H.Sinfelt, *J. Catal.*, **95**(1985)546.

[14] M.G.Mason, L.J.Gerenser and S.T.Lee, *Phys. Rev. Lett.*, **39**(1977)288.

[15] T.Huizinga, H.F.J.van't Blick, J.C.Vis and R.Prins, *Surf. Sci.*, **135**(1983)580.

[16] A.Masson, B.Bellamy, G.Colomer, M.M'bedi, P.Rabette and M.Che, *Proc. 8th Inter. Congr. Catal.*, **IV**(1984)333.

[17] A.Masson, B.Bellamy, Y.Hadj Romdhane, M.Che, H.Roulet and G.Dufour, *Surf. Sci.*, **173**(1986)479.

[18] G.Meitzner, G.H.Via, F.W.Lytle and J.H.Sinfelt, *J. Phys. Chem.*, **96**(1992)4960.

[19] M.G.Samant and M.Boudart, *J. Phys. Chem.*, **95**(1991)4070.

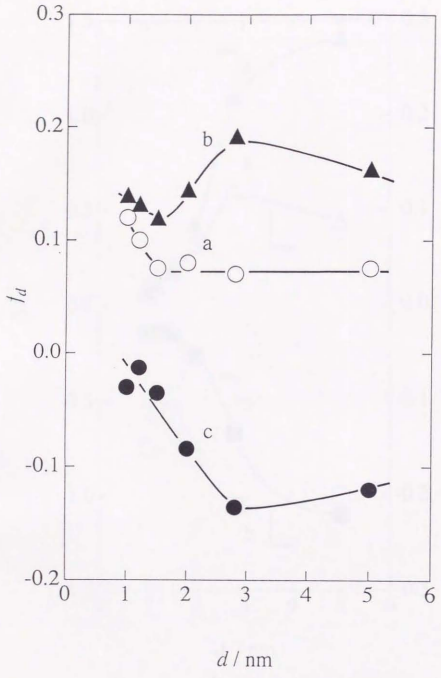

Figure 1. f_d for Pt/SiO_2 as a function of diameter of Pt particles(d); a: under vacuum, b: under 8.0 kPa of ethene, c: under 8.0 kPa of hydrogen.

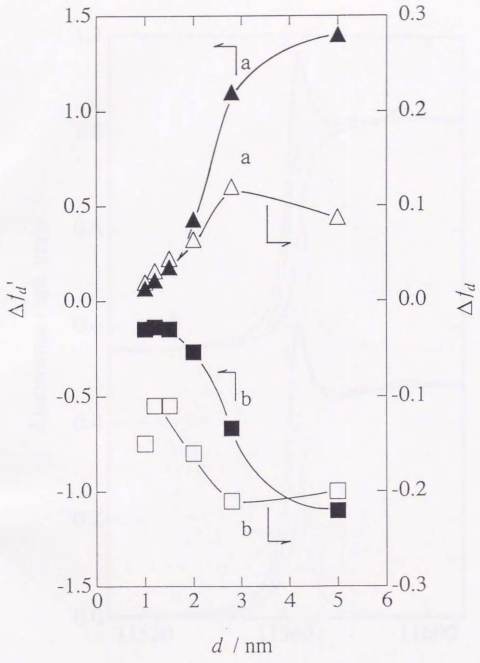

Figure 2. Δf_d(f_d(C_2H_4)-f_d(vacuum) (△) or f_d(H_2)-f_d(vacuum) (□)) as a function of diameter of Pt particles(d); a: under 8.0 kPa of ethene, b: under 8.0 kPa of hydrogen; ▲ and ■ : $\Delta f_d'$(Δf_d divided by the number of adsorbates per Pt).

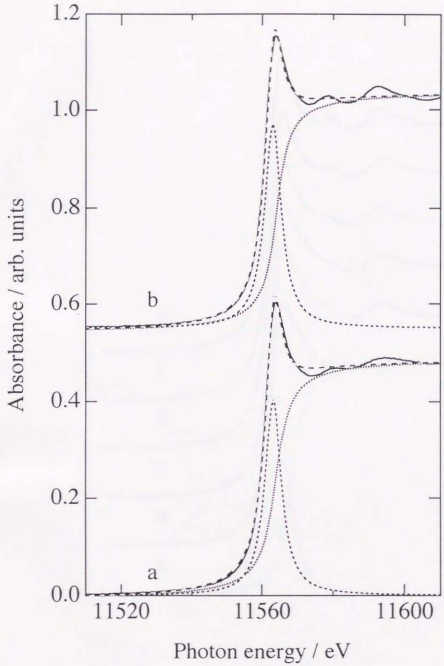

Figure 3. (1)Normalized XANES spectra at L_{III} edge under vacuum (without adsorbed hydrogen); a: d=1.0 nm, b: d=2.8 nm.

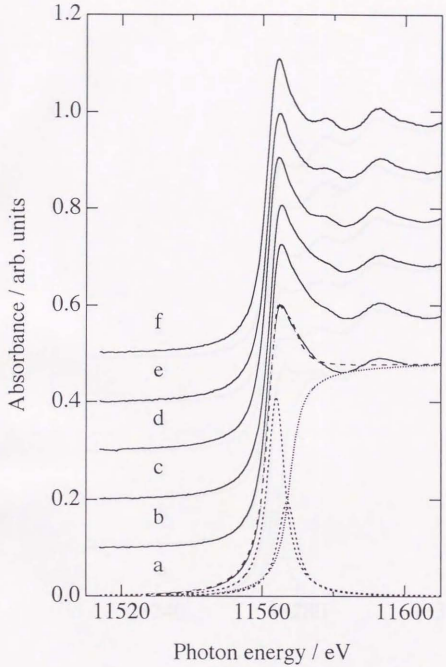

Figure 3. (2)Normalized XANES spectra at L_{III} edge under 8.0 kPa of hydrogen; a: d=1.0 nm, b: d=1.2 nm, c: d=1.5 nm, d: d=2.0 nm, e: d=2.8 nm, f: d=5.0 nm.

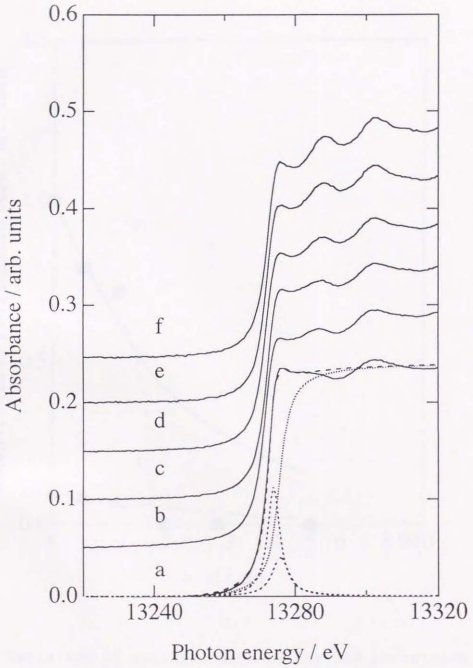

Figure 3. (3)Normalized XANES spectra at L_{II} edge under 8.0 kPa of hydrogen; a: d=1.0 nm, b: d=1.2 nm, c: d=1.5 nm, d: d=2.0 nm, e: d=2.8 nm, f: d=5.0 nm.

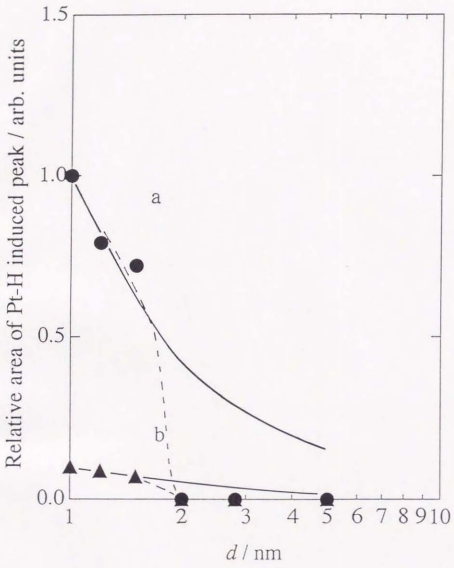

Figure 4. Variation of relative area of the 2nd Lorentzian peak under 8.0 kPa of hydrogen with diameter of Pt particles; a: L_{III} edge, b: L_{II} edge. The solid lines are ones simulated from the ratio of surface Pt atom to bulk Pt atoms as a function of the particle size.

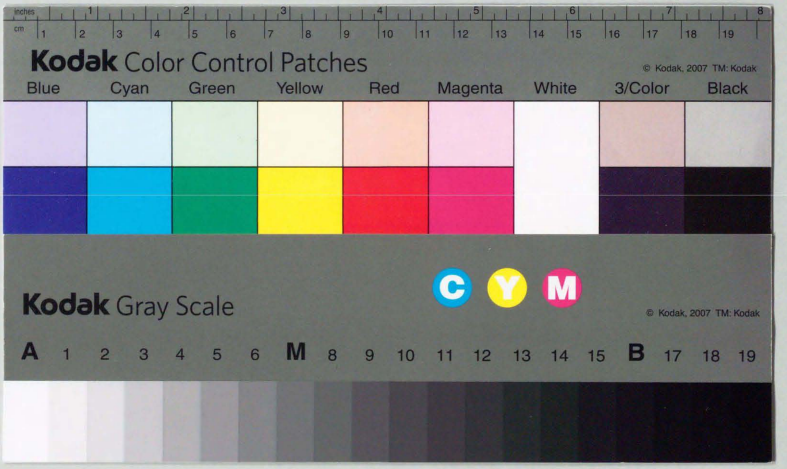
inches
cm
Kodak Color Control Patches
© Kodak, 2007 TM: Kodak
Blue
Cyan
Green
Yellow
Red
Magenta
White
3/Color
Black
Kodak Gray Scale
C
Y
M
© Kodak, 2007 TM: Kodak
A 1 2 3 4 5 6 M 8 9 10 11 12 13 14 15 B 17 18 19